Available online at www.sciencedirect.com
SCIENCE DIRECT®
Journal of Magnetic Resonance 170 (2004) 22–41
JMR Journal of Magnetic Resonance
www.elsevier.com/locate/jmr

Controlling the effects of pulse transients and RF inhomogeneity in phase-modulated multiple-pulse sequences for homonuclear decoupling in solid-state proton NMR

Alexander J. Vega*

DuPont Central Research and Development, Experimental Station, P.O. Box 80356, Wilmington, DE 19880-0356, USA

Received 23 March 2004; revised 20 May 2004
Available online 26 June 2004

Abstract

The effects of pulse imperfections and RF inhomogeneity on NMR spectra obtained with phase-modulated multiple-pulse NMR sequences are analyzed. The emphasis is on the combined effects of frequency offset, RF inhomogeneity, and pulse phase transients. To enable a theoretical description of the transients associated with phase changes under continuous RF irradiation, the nature of the transients is investigated in depth. As monitored in our 300 MHz spectrometer, they are found to be caused by linear elements of the RF circuitry. The validity of their representation as δ-function pulses and the significance of their decomposition into antisymmetric and symmetric components are discussed. A practical method for quantitative control of the antisymmetric phase transients is proposed. The linearity property allows the development of a theoretical description of the spin dynamics caused by the transients. This leads to a vector-Hamiltonian model for phase-modulated Lee–Goldburg experiments. It quantitatively predicts both the frequency shift and the line broadening caused by antisymmetric phase transients and their coupling with RF inhomogeneity. The model is shown to be equally applicable to frequency-switched Lee–Goldburg experiments. A noteworthy discovery is that for a given magnitude of the antisymmetric phase transients a frequency offset exists at which the inhomogeneity broadening is essentially canceled. This explains the common observation that for best resolution one side of resonance is preferred over the other. It also suggests a strategy for enhancing resolution without having to resort to severe sample volume restriction. Numerical calculations verified the theoretical predictions and allowed extension of the model to BLEW-12 and DUMBO-1. Experimental verification is presented. The deviations from theoretical predictions are discussed.

1. Introduction

Following the pioneering work of Lee and Goldburg [1] and Waugh et al. [2], numerous multiple-pulse schemes were invented for decoupling of homonuclear dipolar interactions and achieving high resolution in proton NMR spectra of solid samples. Prominent examples are WHH-4 [2], MREV-8 [3,4], BR-24 [5], BLEW-12 [6], FSLG [7,8], TREV-8 [9], MSHOT-3 [10], PMLG*n* [11–13], DUMBO-1 [14], and *w*PMLG*n* [15]. Since the late 1970s, following the introduction of combined magic-angle-rotation and multiple-pulse (CRAMPS) by Gerstein et al. [16], these methods are nearly always performed together with magic-angle spinning (MAS) for further reduction of line broadenings due to other anisotropic interactions such as chemical-shift anisotropies and heteronuclear dipole interactions. MAS is particularly indispensable in modern heteronuclear double-resonance experiments involving homonuclear proton decoupling in the indirect dimension [17–25]. A general observation has been that RF inhomogeneity contributes considerably to the linewidth [8,26,27], causing the widespread practice of limiting the sample size to small volumes [28,29]. Furthermore, it has been observed that the resolution is often better on one side of resonance than on the other [29]. The aim of this paper is to identify the causes of

* Present address: 1501 Emory Road, Wilmington, DE 19803, USA. Fax: 1-302-695-1664.
E-mail addresses: alexander.j.vega@usa.dupont.com, lexvega@comcast.net.

1090-7807/$ - see front matter © 2004 Elsevier Inc. All rights reserved.
doi:10.1016/j.jmr.2004.05.017

these and similar phenomena, to quantify them, and to learn how to control their impact.

The multiple-pulse schemes are periodic radiofrequency (RF) irradiation sequences of varying amplitude and phase. They require observation of the NMR signal after integer numbers of pulse cycles. When the sequence contains windows, this can be done stroboscopically, otherwise it must be in 2D fashion. As a side effect the multiple-pulse methods reduce the chemical shifts by a scaling factor between 0.45 and 0.6 [29]. Most of the pulse cycles are designed with the objective to decouple homonuclear interactions in static samples. MAS interferes with the averaging scheme of these pulse cycles because it modulates the angles θ between the internuclear vectors and the magnetic field, thereby adding an additional time dependence to the $(1-3\cos^2\theta)$ multipliers of the dipolar interaction. To minimize the impact of the rotation-induced fluctuations on the multiple-pulse experiments mentioned above, it is required that the frequency ω_{MP} of the pulse cycles is much larger than the sample rotation frequency ω_R. For that reason the windowless sequences, i.e., those that modulate the phase while keeping the RF irradiation continuously on with a constant amplitude ω_1, are preferred in CRAMPS experiments. They include the pulse cycles BLEW-12 [6] and DUMBO-1 [14] (both having cycle time $t_c = 6\pi/\omega_1$), and FSLG [7] and PMLGn [11] (both having $t_c = 4\pi\sqrt{2/3}/\omega_1 = 3.27\pi/\omega_1$). Synchronization between the two frequencies ($n\omega_R \cong m\omega_{MP}$) should also be avoided to prevent interference [12]. Following an alternative approach, multiple-pulse/MAS experiments have been designed where the spin and space averaging reinforce each other [30,31]. The concepts developed in this paper also apply to those pulse sequences.

This paper is concerned with residual line broadenings and frequency shifts that affect the scaled isotropic-shift peaks in the CRAMPS spectra of windowless sequences. These artifacts are caused by incomplete averaging of the dipole interaction and by pulse-sequence imperfections such as timing errors, RF amplitude misadjustment, RF inhomogeneity, phase misadjustment, finite pulse widths in cases where the ideal sequence calls for δ-function pulses, and the so-called pulse transients, which are RF distortions that accompany sudden changes in amplitude and/or phase. Rhim et al. [32] developed a comprehensive theory for these effects in static multiple-pulse experiments [27]. Their results are, however, not fully applicable to CRAMPS, because the residual dipolar broadening due to pulse imperfections is much smaller under MAS conditions than it would have been under static conditions, as has been pointed out recently [12,33]. In fact, CRAMPS is quite tolerant to the deliberate introduction of non-ideal elements in the pulse sequence, such as large-step phase modulation in FSLG [12] and the insertion of an observation window [15]. In this paper we will refer to the residual dipolar broadenings and other T_2-type effects as the 'natural linewidth.'

We thus focus our attention on a systematic investigation of the major remaining spectral distortions, i.e., those due to the pulse imperfections and their interplay with the chemical-shift offset, without consideration of the dipolar interaction. Specifically, we will consider pulse transients and deviations of the RF amplitude from its ideal value. The other pulse errors mentioned above do not warrant an in-depth analysis. For instance, the only manifestation of timing errors that we could identify is the short time lapse between the programmed phase shifts and their actual execution as experienced by the nuclei. It can easily be accounted for in the pulse program and does not pose spectral problems. Phase errors will not be considered either, because they are virtually non-existent in modern spectrometers. Phase transients were the subject of theoretical and experimental observations recently reported by Bosman et al. for wPMLG experiments [34]. The present work can be seen as an extension of their effort.

The theoretical analysis of the spin dynamics can be kept rather simple. To begin with, the exclusion of dipolar interactions frees us from having to work with a density-matrix formalism. It is sufficient to follow the precessions and nutations of the spin-1/2 magnetization in Cartesian space in the presence of magnetic fields. Moreover, since none of the considered interactions depend on the orientation, MAS is inconsequential so that the only periodicity to be taken into account is that of the multiple-pulse sequence. Hence, calculating the net rotation operator over one irradiation cycle and dividing it by the cycle time constitutes a full characterization of effective Hamiltonian, which can then be represented as an effective magnetic field in the rotating frame. Although approximations are invoked, there is no reason to apply average-Hamiltonian theory [26,27] or Floquet formalism [35].

In Section 2 we attempt to provide convincing evidence that pulse distortions follow the rules of linear response theory and that their size can be controlled, at least in our 300 MHz spectrometer. This conclusion is based on phenomenological observations rather than on mathematical analysis of AC currents in RF circuits. The linear nature of the transients then enables the calculation of the effects of pulse transients and RF misadjustment, to be described in Sections 3 and 4. It is first worked out in a theory for the PMLG sequences, which have the particular advantage that the spin dynamics can readily be visualized in a pictorial description of effective magnetic fields. Those results are then verified and expanded in the next section, where numerical results of the effective Hamiltonians for PMLG, BLEW-12, and DUMBO-1 are presented. In Section 5 the theory is compared with PMLG measurements. In Section 6 the discrepancies between theory and

experiment are discussed and a practical strategy for controlling the effects is proposed.

2. Nature of the transients

We begin with an investigation of the nature of the phase transients. They are caused by elements of the RF electronics that transform the square pulses programmed by the pulse-sequence software into phase- and amplitude-distorted RF profiles experienced by the nuclei in the sample coil. Most of these elements produce linear distortion effects in the sense that the response of the sum of input pulses is the sum of the individual responses. To this class belong capacitors, inductances, resistors, transmission lines, filters, and linear amplifiers. Other elements, such as diodes, non-linear amplifiers, digital circuitry of the pulse shaping electronics, and construction materials leading to probe ringing, can produce a non-linear response. For a pulse of sufficiently long duration the distortion consists of two distinct transient events at the leading and trailing edges. If we decompose the time profile of a distorted RF pulse into two quadrature phase components, we find that the component having the same phase as the middle section of the pulse resembles the ideal square shape albeit with sloping edges, whereas the 90°-out-of-phase component consists of two short pulses at the edges. A hallmark of linear-response pulse distortions is that the leading and trailing transients are opposites of each other. This is readily appreciated when we picture two consecutive equivalent rectangular pulses having the same RF amplitudes, phases, and durations. If the delay between the pulses is reduced to zero, they merge into one continuous pulse with obviously no transient effects at the point of joining. Since linear response implies that the (vanishing) intermediate transient is the sum of the trailing transient of the first and the leading transient of the second pulse, the two must be the inverses of each other. (See Appendix A for the discussion of a subtle difficulty with this argument.)

Previous theoretical investigations of pulse transients in NMR were mainly based on the theoretical analysis of AC currents in circuits consisting of linear components and, consequently, led to similar conclusions. Principal among those are analytical expressions for a tuned RLC circuit by Ellett et al. [36], a numerical analysis of the combined resonant circuits of the power amplifier and the probe by Vaughan et al. [37], and analytical expressions describing an impedance-matched probe circuit by Barbara et al. [38]. Caravetta et al. [39] used a similar model to study the effect of pulse transients on some homonuclear recoupling pulse sequences. One objective of the presentation in this section is to demonstrate experimentally that in our spectrometer the pulse transients are indeed dominated by linear distortion effects. The most direct way of measuring the RF currents in the coil is to detect the signals picked up by a small antenna placed nearby [37,39]. However, rather than resorting to this invasive method and having to take into account the extra distortions introduced by the measurement itself, we chose to characterize the transients indirectly through their effects on the NMR signal of a single spin species on exact resonance.

An example of how a profile of a linearly distorted pulse could look like is shown in Fig. 1A [36,38–40]. It pictures a 2.4-μs-long ideal pulse distorted by equal but opposite transients at the leading and trailing edges. Its in-phase transients are given by $\pm\exp(-t/\tau_d)$ and its 90°-out-of-phase transients by $\pm 2[1-\exp(-t/\tau_r)]\exp(-t/\tau_d)$. They may be called 'amplitude transients' and 'phase transients,' respectively. The rise and decay times τ_r and τ_d were both assigned the value of 0.3 μs in accordance with the Q-factor of our probe circuit, which is about 300 (see Section 7), implying that the relaxation time of the tuned electronic circuit is $2Q/\omega_0 \sim 0.3$ μs, ω_0 being the resonance frequency in s^{-1} [36,41]. We are careful not to call these transients antisymmetric, because that would imply the existence of a center of inversion at the midpoint of the pulse. Borrowing from crystallographic terminology, the symmetry is more appropriately described as that of a glide plane. In principle, the transients can be decomposed into symmetric and antisymmetric components with respect to

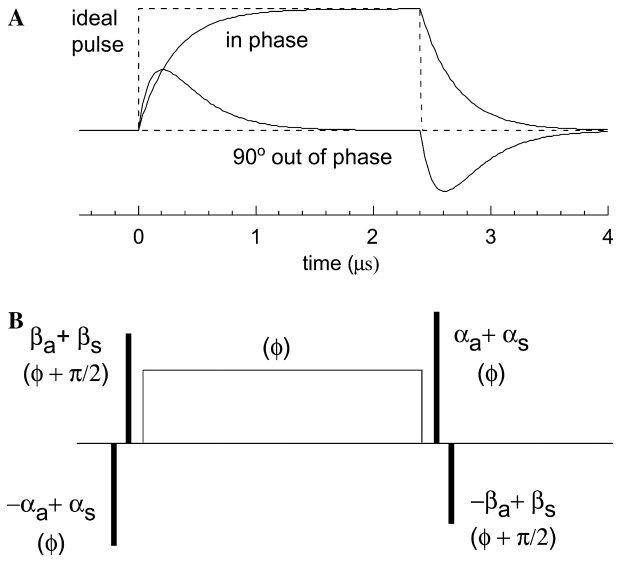

Fig. 1. (A) An example of how the in-phase and 90°-out-of-phase components of a linearly distorted square pulse of length 2.4 may look like. The profiles of the transients are combinations of rising and decaying exponentials as described in the text. (B) The δ-function model for the transients accompanying a square pulse of phase ϕ. α_s and α_a are the flip-angles of the symmetric and antisymmetric components of the in-phase transient pulses, while β_s and β_a are the flip-angles of the symmetric and antisymmetric components of the out-of-phase transient pulses, respectively. The phases of the pulses are indicated in parentheses.

the midpoint of the pulse, but as we shall see shortly, it has little practical significance.

In the spin-dynamics theory to be developed below we will ignore the time duration of the transients. This means that we approximate a pulse as a rectangle accompanied by transients that are represented by δ-function pulses just before and after its rising and trailing edges (Fig. 1B). Two separate pairs of δ-function pulses are needed to represent the in-phase and out-of-phase components of the transients. We further decompose each δ-function-pair into symmetric and antisymmetric components with respect to the center of the pulse. Accordingly, the flip angles of the leading and trailing amplitude transients will be designated as $\alpha_s - \alpha_a$ and $\alpha_s + \alpha_a$, respectively. Similarly, the leading and trailing phase transients will have flip angles $\beta_s + \beta_a$ and $\beta_s - \beta_a$. As to the notation of the δ-function flip angles we will adhere to the following sign convention. For the antisymmetric component of phase transients accompanying a pulse of phase ϕ, the leading and trailing transients have identical flip angles β_a and opposite phases $\phi + \pi/2$ and $\phi - \pi/2$, respectively. (This is equivalent to saying that the trailing transient has inverted flip angle $-\beta_a$ and non-inverted phase $\phi + \pi/2$.) For the symmetric component both have flip angle β_s and phase $\phi + \pi/2$. β_a and β_s may be positive or negative. In the case of the amplitude transients, we note that the leading transient is always opposite to the ideal RF irradiation (see Fig. 1A). This leads the convention that the flip angles of the leading and trailing antisymmetric amplitude transients will be designated $-\alpha_a$ and α_a, respectively. The effect of δ-function transients on the NMR signals following pulses of flip angles 90°, 180°, and 360° can easily be evaluated by executing the nutations of the consecutive components of the pulses. For later reference the resulting signals are described in Table 1 together with the signals following pairs of isolated 180° pulses with equal or opposite phases.

In addition to demonstrating the linear behavior of the transients in our spectrometer, we also intend to test the δ-function assumption. It is theoretically justified by the smallness of the nutation angles caused by the RF irradiation over the total duration of the transients. For instance, if the 2.4 μs pulse shown in Fig. 1A were a 90° pulse, the integrated flip angle of each individual in-phase or out-of-phase transient event would be 11°. As we shall see, in practice the phase transients are smaller than that. Although rotations about axes of different orientations are in general notoriously non-commutative, this is not as serious a complication when the rotations are over small angles. In such cases the order in which the rotations occur is of little consequence. Therefore, the successive infinitesimal nutation events over the course of the transients may be approximated by a single event at one particular time. In this approximation the flip angles of the leading edge δ-function transients of a pulse are defined as the integrals of the corresponding transient profiles. In the δ-function model of linear transients the flip angles are thus necessarily antisymmetric, so that α_s and β_s must be zero.

This was tested numerically for the pulse profile shown in Fig. 1A. We assigned to it the RF amplitude appropriate for a 2.4 μs 90° pulse and calculated its effect on a magnetization vector originally pointing along z, by numerically performing the consecutive nutations of small time increments. In particular, we calculated the resulting NMR signals following 4.8 and 9.6 μs pulses and compared the results with the entries in Table 1 for 180° and 360° pulses so that we could estimate the equivalent antisymmetric and symmetric δ-function transients. We found β_a to be 11°, indeed matching the integrated flip angle of the profiled transient. It can be scaled by modifying the coefficient 2 in front of the expression of the out-of-phase component. Furthermore, we found β_s and α_s to be less than 0.1°, thus supporting the δ-function approximation. However, β_s and α_s can

Table 1
Amplitudes and phases of on-resonance NMR signals generated by RF pulses accompanied by antisymmetric or symmetric δ-function transients

Pulses[a]	Antisymmetric transients		Symmetric transients	
	Signal ampl.	Signal phase	Signal ampl.	Signal phase
Phase transients				
90_x	~ 1	$\sim\beta_a$	~ 1	$\sim\beta_s$
180_x	$\sin(2\beta_a)$	$\pi/2$	0	—
360_x	0	—	$\sin(2\beta_s)$	$\pi/2$
180_x, 180_x	0	—	0	—
180_x, 180_{-x}	$\sin(4\beta_a)$	$\pi/2$	0	—
Amplitude transients				
90_x	1	0	~ 1	0
180_x	0	—	$-\sin(2\alpha_s)$	0
360_x	0	—	$\sin(2\alpha_s)$	0
180_x, 180_x	0	—	$\sin(4\alpha_s)$	0
180_x, 180_{-x}	0	—	0	—

[a] The 180_x, $180_{\pm x}$ pulse pairs are separated by a time delay.

both be made as large as $\beta_a/3$ in magnitude by shortening τ_r to 0.05 μs. Thus depending on the details of the shapes of the profiles, the finite width of the transients can contribute to symmetric δ-function transients after all. This is a higher-order effect caused by the non-commutativity of the consecutive infinitesimal precession events: Although the leading transient is equal to the inverted trailing transient, its effect on magnetization precession is the exact opposite of that of the trailing transient only in first-order approximation. Higher-order corrections depend on the circumstances in which the transients occur. Since the leading transient is actually a negative irradiation coexisting with the full ideal pulse irradiation whereas the trailing transient stands alone (see Fig. 1A), they do not produce exactly opposite precession motions. On the other hand, in a pulse sequence where the trailing transient also coincides with full RF irradiation of identical phase, as in the above-mentioned thought experiment of two back-to-back identical pulses, it counteracts the leading transient exactly.

For transients caused by linear pulse distortions we may thus conclude that in first-order approximation the transients can be represented by δ-function pulses that are antisymmetric and independent of the RF irradiation immediately preceding and following the pulse. Higher-order effects, which do depend on the details of the irradiation scheme, can introduce symmetric δ-function transients. In addition, the apparent flip angles of the antisymmetric transients can vary slightly with the details of the sequence. In principle, each pulse sequence requires its own exact definition of the sizes of the antisymmetric and symmetric components. For instance, Rhim et al. in their analysis of error Hamiltonians caused by pulse imperfections in multiple-pulse experiments, used definitions appropriate for isolated 90° pulses [27,32]. The following simple NMR measurements were done to test the reliability of a first-order δ-function approach in experimental situations.

The left column of Fig. 2 shows the Fourier transformed on-resonance proton signals of hexamethylbenzene (HMB) spinning at 16 kHz following pulses of widths 2.4, 4.8, and 9.6 μs having an identical amplitude, which was adjusted to produce a 360° pulse at 9.6 μs. The spectra were phased uniformly such that the 180° pulse gave a pure dispersion lineshape in accordance with the predicted phase listed in Table 1. The lineshapes show the simultaneous signatures of antisymmetric and (smaller) symmetric phase transients: a slight phase shift at 90°, a substantial quadrature signal at 180°, and a smaller quadrature signal at 360°. The sizes of the antisymmetric and symmetric contributions were estimated at $\beta_a = -6°$ and $\beta_s = 2°$, respectively. As mentioned above, the small symmetric contribution is a higher-order effect related to the particular shape of the transient profiles. However, it does not contradict the linearity

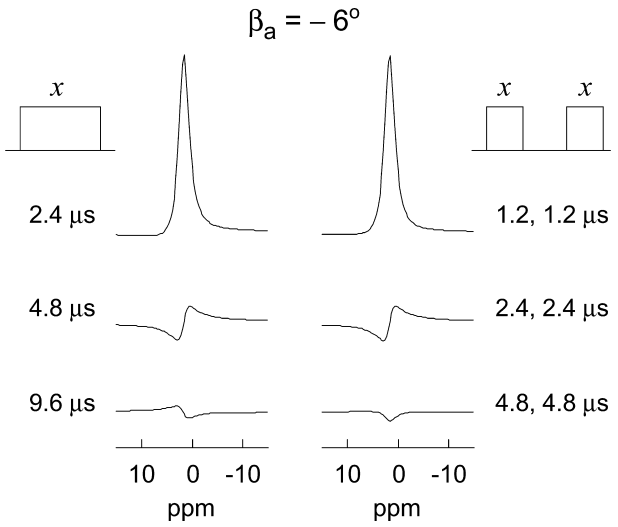

Fig. 2. Fourier transformed on-resonance MAS signals of HMB spinning at 16 kHz following a single pulse (left) or two identical pulses separated by 5 μs (right). The pulse lengths are as indicated. The RF amplitude was the same in all cases. It was calibrated to give a 360° pulse of 9.6 μs length. Transmitter amplifier and probe were tuned to produce antisymmetric phase transients of flip angle $\beta_a \approx -6°$.

principle. The right column of Fig. 2 shows the results of similar experiments, modified such that the pulses were split in the center with insertion of a 5 μs delay. We see that the NMR signal following the split 180° pulse is hardly affected by the insertion of the gap, demonstrating that to a good approximation the trailing transient of the first pulse cancels the leading transient of the second pulse, even though they occur under different conditions. The split 360° pulse does not reflect the existence of symmetric phase transients, as expected for additivity in two consecutive 180°'s (see Table 1). On the other hand, the small negative absorption peak in the right bottom spectrum of Fig. 2 indicates the presence of a small symmetric amplitude transient, although it could also be due to RF amplitude instability (see Section 7).

Following the suggestions of previous investigators [36–39], who observed that the size of pulse transients is sensitive to adjustments of capacitors of the RF circuits, we were able to retune the spectrometer to a configuration where β_a nearly vanishes. An account of how this can be done in a controlled manner is given below. With β_a set to a very small value, the on-resonance experiments of Fig. 2 were repeated. The results, shown in Fig. 3, show that the effects of the transients are indeed greatly reduced and that insertion of a gap remains inconsequential. Interestingly, the symmetric and antisymmetric transients are nulled simultaneously, suggesting that they are manifestations of the same RF distortion phenomenon.

Thus far we considered phase-transient combinations of pulses with identical nominal phases. We now turn

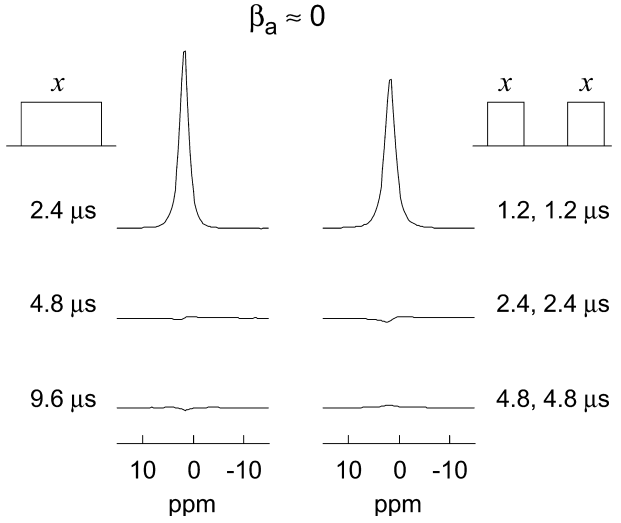

Fig. 3. The experiments of Fig. 2 repeated with a spectrometer tuning configuration that produces essentially no transients.

our attention to transients associated with 180° phase shifts. Spectra were first obtained with the spectrometer tuned for negligibly small phase transients ($\beta_a \approx 0$). The left column of Fig. 4 shows Fourier transformed signals following a pulse having a total length of 9.6 μs (corresponding to two 180°s), consisting of two portions with phases x and $-x$, which were *programmed* such that the first portion was slightly shorter than the second as indicated in the figure. The right column shows the signals of two pulses separated by 5 μs. Their phases were also x and $-x$ and their pulse widths were as indicated in the figure. Comparison of the left and right columns shows

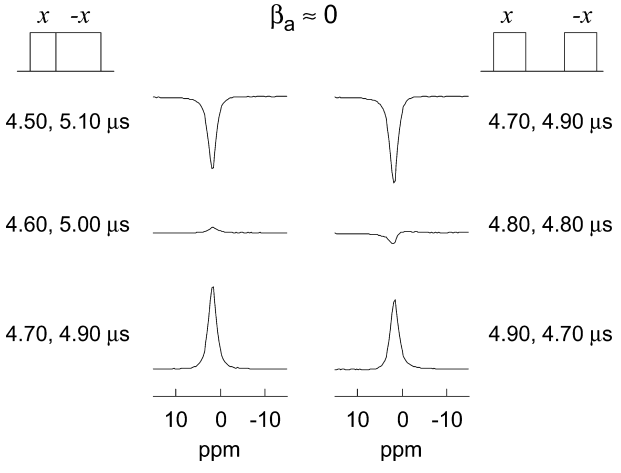

Fig. 4. Fourier transformed on-resonance MAS signals of HMB spinning at 16 kHz following two pulses with opposite phase with no separation (left) or a 5 μs separation (right) between the pulses. The total length of the double pulse is twice that of a 180° pulse (2×4.8 μs) in all cases. The pulse lengths are as indicated. The RF amplitude was the same in all cases. It was calibrated to give a 180° pulse of 4.8 μs length. Transmitter amplifier and probe were tuned to produce essentially no antisymmetric phase transients.

that the phase shift as experienced by the nuclei in the coil comes 0.20 μs after it has been programmed in the pulse sequence. In the sense of the transients classification outlined above, this delay can be viewed as an example of a 'non-linear pulse distortion' caused by the electronics. Fortunately, it can easily be compensated by programming the phase shifts with the appropriate preset delay. Another important observation is that the signals in the left column of Fig. 4 show no evidence of additional nutations due to phase transients that could have occurred at the moment of the phase shift. Similarly, when the experiment of Fig. 4 was repeated with a spectrometer setup that gave substantial antisymmetric transients ($\beta_a = -6°$), the signals obtained with and without an intervening delay were essentially identical to each other (see Fig. 5). We thus find again that the combined transient at a 180° phase shift under continuous RF irradiation can to a good approximation be described by a simple addition of the transients of the trailing and leading edges of the individual pulses before and after the shift. We note that the effect of antisymmetric transients in the case of a $180°_{x}$, $180°_{-x}$ pulse pair is substantial, since it induces a $4\beta_a$ overall nutation of the magnetization, leading to a quadrature signal amplitude of $\sin(4\beta_a)$ (see also Table 1).

The experiments just described give evidence that, in addition to a 0.2 μs phase-shift delay and occasional minor deviations, the phase transients of our spectrometer are by and large antisymmetric and additive. All evidence confirms that they are the result of linear pulse distortions. Admittedly, we have proven it only for phase shifts that are either 0° or 180°. For smaller phase shifts, like those that occur in the PMLG sequence, we were able to verify that the required phase preset time is also about 0.2 μs (data not shown). However, in order to establish the absence of phase transients that could prevail in addition to those determined by the additivity

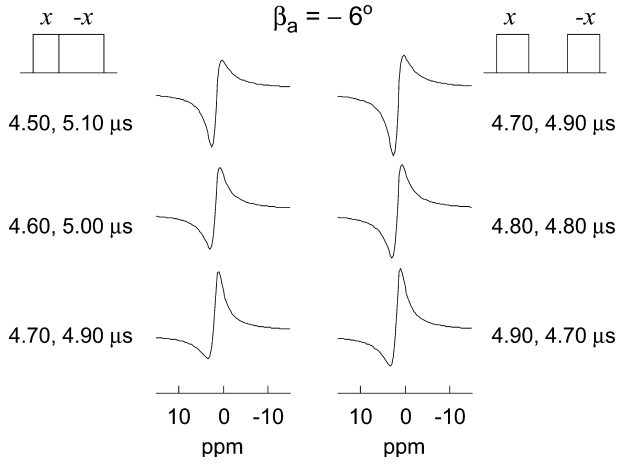

Fig. 5. The experiments of Fig. 4 repeated with a spectrometer tuning configuration that produces antisymmetric phase transients of flip angle $\beta_a \approx -6°$.

principle, sequences consisting of many more than two pulses are needed to measure the effects precisely. We did not attempt to do this in a separate experiment. Instead, the degree of success with which the antisymmetric δ-function model predicts the experimental results of the PMLG cycle (results to be presented below) will serve that purpose. Whereas the measurements reported above were obtained with the power amplifier operating in class AB, we also performed them in class C and found identical results. Hence, although the class-C amplifier has non-linear character, it does not seem to introduce non-linear or even linear pulse distortions beyond those generated in class AB.

The linear and additive character of the transients has several important consequences. First, the transients are mainly antisymmetric as mentioned above. Second, additivity negates the benefit of the insertion of gaps in the pulse sequence for the purpose of reducing transients associated with phase shifts. Third, additivity allows calculation of the flip angle and the phase of the combined antisymmetric transients accompanying a phase shift during continuous RF irradiation. This calculation uses the fact that two simultaneous pulses of equal flip angle θ and phases ϕ_1 and ϕ_2 are equivalent to a single pulse of flip angle $\theta_{\text{eff}} = 2\theta\cos[(\phi_2 - \phi_1)/2]$ and phase $\phi_{\text{eff}} = (\phi_1 + \phi_2)/2$. The coinciding individual trailing and leading antisymmetric phase transients at a point in time where the RF phase switches from ϕ to ψ have phases $\phi_1 = \phi - \pi/2$ and $\phi_2 = \psi + \pi/2$. From this it follows that the combined antisymmetric transient has flip angle

$$\beta_{\text{eff}} = 2\beta_{\text{a}}\sin[(\phi - \psi)/2] \tag{1}$$

and phase

$$\phi_{\text{eff}} = (\phi + \psi)/2. \tag{2}$$

As may have been expected intuitively, the phase of the combined transient pulse is thus the average of the phases before and after the switch, while its size scales with the phase difference. An additional remarkable finding is that according to Eq. (1) the sign of the transient depends on whether ϕ is larger or smaller than ψ. An alternative way of expressing this is to say that the sign of β_{eff} is always that of β_{a} while ϕ_{eff} is incremented by π in cases where the phase shift is positive. This will turn out to be of crucial importance for the effect of phase transients on the performance of PMLG sequences. A special case encountered in PMLG is a 180° phase shift under continuous RF irradiation. It can be treated in two alternative ways, by choosing either $\psi = \phi + \pi$ or $\psi = \phi - \pi$. It is reassuring to note that the two alternatives lead to the same result: $\beta_{\text{eff}} = 2\beta_{\text{a}}$ and $\phi_{\text{eff}} = \phi - \pi/2$.

The antisymmetric in-phase or "amplitude" transients can be treated similarly. When they coincide between back-to-back pulses of phases ϕ and ψ, their combined effect is represented by a δ-function pulse with effective flip angle

$$\alpha_{\text{eff}} = 2\alpha_{\text{a}}\sin[(\phi - \psi)/2] \tag{3}$$

and effective phase

$$\phi_{\text{eff}} = (\phi + \psi)/2 + \pi/2, \tag{4}$$

which is similar to the effective antisymmetric phase transient (Eqs. (1) and (2)) in that it scales with the phase difference and inverts its sign when $\phi < \psi$. However, in contrast to the phase transient it is 90° out of phase with the average of ϕ and ψ.

The symmetric phase transients β_{s} and the symmetric amplitude transients α_{s} present a problem if we wish to treat their combined effects between back-to-back pulses in a similar way because, as discussed above, they manifest themselves differently in different circumstances. For instance, between pulses of equal phase they cancel each other. Therefore, we feel safe to ignore the symmetric transients associated with the small phase shifts that are prevalent in PMLG sequences. They are also irrelevant at 180° phase shifts, because even if they were included as β_{s} or α_{s} pulses, the two coinciding transient pulses would have opposite phase thus cancel each other. In any case, symmetric transients are higher-order effects, which we intend to neglect in the theoretical model. Moreover, as we shall see below in the numeric simulations, incorporating them in the model does not lead to changes in the effective Hamiltonian.

A fourth consequence of the fact that the transients are generated by linear components of the electronics is that changing the values of the components, notably the capacitors, will affect the sizes of the transients [36–39]. Here we show how this can be done in a controlled manner. It is obviously not possible to measure the exact values of the tuning and matching capacitors in the tuned LC circuits of the amplifier and the probe. However, we can efficiently quantitate the overall configuration of an impedance-matched circuit by recording its resonance frequency. In doing so for the NMR spectrometer we have to keep track of three frequencies. One frequency is ν_{NMR} at which the on-resonance NMR experiment is done. The second frequency is ν_{trans} at which the transmitter amplifier gives maximum output into a 50 Ω load. The third frequency is ν_{probe} at which the probe gives minimum reflected power as measured with a directional coupler. Since we have no leeway in the choice of ν_{NMR} unless the magnetic field is changed, we measured β_{a} as a function of ν_{trans} and ν_{probe}. The probe configuration is reproducibly controllable to a high degree of accuracy in this way, because the positions of both the matching and tuning capacitors are precisely determined by ν_{probe}. On the other hand, the configuration of the transmitter is only crudely defined by ν_{trans}. For that reason, we performed the experiments in sets where the transmitter knobs were kept in fixed

positions, while ν_{probe} was varied. The measurements were done on resonance with a 'flipflop' pulse sequence consisting of 180° pulses with alternating phase: $180°_x$, $180°_{-x}$, $180°_x$, $180°_{-x}$, etc. The signal was detected stroboscopically after each second pulse. The data reflect a precession about the y-axis with $4\beta_a$ phase increment between consecutive points (compare Table 1 for $180°_x$, $180°_{-x}$). Thus the FID is a sine wave without dc offset. Fourier transformation gives a frequency from which the flip angle β_a and its sign can readily be deduced. Results of these measurements, performed on HMB spinning at 16 kHz with 35 μs delays between the 180° pulses, are shown in Fig. 6. Using these calibration curves we were able to reproduce β_a within 0.3° as long as both the sample and the transmitter settings remained unchanged. Amplitude transients are expected to be much less sensitive to probe tuning. In particular, they cannot be nulled out because it will always take a certain amount of time, dictated by the Q-factor, for the pulse to turn on or off. However, since it will be shown below that amplitude transients have no first-order effect on the performance of multiple-pulse experiments, this is of minor concern. The ν_{probe} ranges of the calibration curves in Fig. 6 are terminated at minimum and maximum tuning frequencies beyond which β_a measurements became erratic. We suspect that when the probe is severely detuned, the δ-function description of the phase transients loses its validity.

A fifth consequence of linearity is that β_a is proportional to ω_1. To verify this, some of the measurements of Fig. 6 were repeated with half the RF amplitude (180° pulses of 9.6 μs instead of 4.8 μs). It resulted in a $46 \pm 6\%$ reduction of β_a, which we consider to be satisfactory. It follows that the ratio β_a/ω_1 is a characteristic parameter of the spectrometer tuning. It can be expressed in units of °/kHz or in rad/(rad s^{-1}) = s, where 1 μs corresponds to 0.36°/kHz. In the examples of Fig. 6 the phase transients were as large as 0.077°/kHz or 0.21 μs. The physical significance of the time dimension of this property is that it would be the duration of a transient pulse if it were rectangular in shape and had the same amplitude as the bulk of the pulse (compare Fig. 1A).

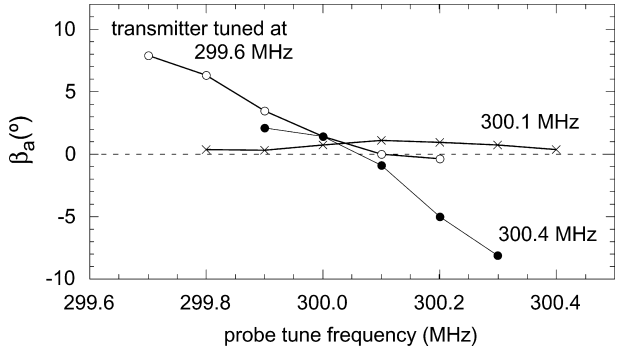

Fig. 6. Flip angle of antisymmetric phase transients as function of probe tuning frequency, measured for three tuning configurations of the transmitter amplifier and at an NMR resonance frequency of 300.12 MHz.

The profiles of Fig. 1A seem to suggest that when pulses become shorter than 1 μs, the δ-function model gradually begins to lose validity, because the leading and trailing transients start running into each other. Since they are of opposite sign, the equivalent β_a values for short pulses are expected to be greatly reduced. Nevertheless, we can argue that the model of δ-function transient pulses will remain largely valid with undiminished β_a nutation angles even when the pulses are very short. This is a result of the fact that short pulses represent small flip angles, resulting in commutative spin rotations. Hence, although the sequences of the nutation events related to the pulse and its accompanying transients take place simultaneously over a period of several hundred ns, their net total nutation is essentially independent of the order in which they occur. Therefore, we expect the model developed in the following section for phase transients in phase-modulated Lee–Goldburg sequences (consisting of relatively long elementary pulses) to be equally applicable to the FSLG sequence, which is identical to PMLGn in the limit of very large n. In fact, it is shown in Appendix B that in the limit of a smooth phase ramp ($n \to \infty$) the first-order RF distortion is identical to that of stepped phase increments.

3. Theory of frequency shifts in PMLG and FSLG

The pulse cycle of frequency-shifted Lee–Goldburg (FSLG) NMR [7] consists of two RF pulses having equal amplitude ω_1 and duration τ_{LG}, but having different frequencies $\omega_0 + \Delta\omega_{LG}$ and $\omega_0 - \Delta\omega_{LG}$ and different phases 0° and 180° [7]. An equivalent description states that the two pulses have identical frequency ω_0, but that their phases $\phi(t)$ are time dependent. In the first half of the cycle the phase is ramped up linearly from $\phi(0) = 0$ to $\phi(\tau_{LG}) = \phi_{LG} = 2\pi/\sqrt{3} = 207.85°$ and in the second half it is ramped down from $\phi(\tau_{LG}) = \pi + \phi_{LG}$ to $\phi(2\tau_{LG}) = \pi$. For suppression of homonuclear dipole interactions it is ideally required that

$$\omega_1 = \Delta\omega_{LG}\sqrt{2} \tag{5}$$

and

$$\Delta\omega_{LG}\tau_{LG} = \phi_{LG} = 2\pi/\sqrt{3}. \tag{6}$$

The PMLGn experiment is identical to phase-modulated version of FSLG with the only difference that the phase ramping is programmed in n discrete steps [11]. The practical implementation of FSLG is often like PMLGn with a large number of small steps [42]. The pulse-program code ensures that the required relationship of Eq. (6) between $\Delta\omega_{LG}$ and τ_{LG} is automatically satisfied.

However, the LG matching condition between the RF amplitude ω_1 and the irradiation offset $\Delta\omega_{LG}$ (Eq. (5)) is not always met, as it is subject to RF misadjustment and RF inhomogeneity across the sample volume.

As mentioned in Section 1, we restrict the analysis of the spin dynamics to the description of precessions and nutations of the magnetization vector in Cartesian space. The most convenient way of doing this is by transformation to a coordinate frame that in the first half of the cycle rotates about the static magnetic field (the z direction) at a frequency $\omega_0 + \Delta\omega_{LG}$ with respect to the laboratory frame and continues to rotate in the second half at frequency $\omega_0 - \Delta\omega_{LG}$, and so on. We refer to it as the 'rocking rotating frame.' If we restrict the measurements to stroboscopic detection after the completion of integer numbers of FSLG cycles, it is as if the data are obtained in the 'normal' rotating frame of frequency ω_0 because the two consecutive extra rotations at frequencies $\Delta\omega_{LG}$ and $-\Delta\omega_{LG}$ compensate each other. The precessional motion of spins that are on resonance at the carrier frequency ω_0 is as follows. In the first half of the cycle they precesses about a so-called vector-Hamiltonian composed of two components, one being a vector of size ω_1 along x and the other a vector of size $-\Delta\omega_{LG}$ along z. The latter compensates for the difference between the resonance frequency ω_0 and the frequency $\omega_0 + \Delta\omega_{LG}$ of the rocking rotating frame. (Note that by assuming that ω_1 remains exactly parallel to x, the finite step sizes of the phase increments in PMLG are ignored.) This vector-Hamiltonian is represented in the left diagram of Fig. 7 as the LG vector. In the second half of the cycle, the directions of $\Delta\omega_{LG}$ and ω_1 are inverted so that they point along $+z$ and $-x$, respectively, giving an LG vector in the opposite direction, as shown in the second drawing of Fig. 7. The consecutive precessions about the two LG vectors compensate each other irrespective of whether the LG conditions Eqs. (5) and (6) are met.

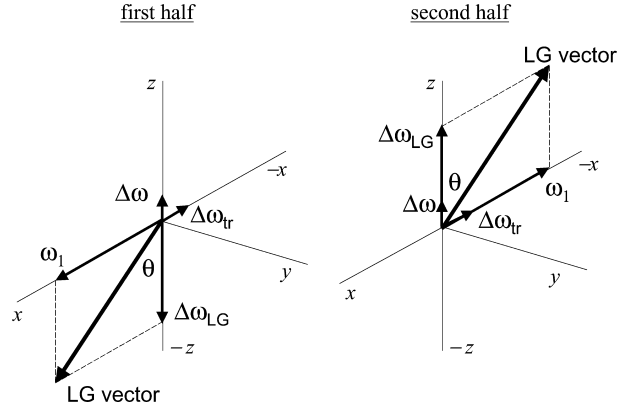

Fig. 7. Arrows representing components of the magnetic field experienced by nuclear spins in the rocking rotating frame. The left and right diagrams are for the first and second halves of the FSLG cycle, respectively. $\Delta\omega_{LG}$ is the difference between the frequency of the rocking rotating frame and the conventional rotating frame. ω_1 is the applied RF field. The LG vector is the sum of the $\Delta\omega_{LG}$ and ε_1 vectors. $\Delta\omega$ is the frequency offset of the nuclear resonance frequency. $\Delta\omega_{tr}$ is the average RF field due to antisymmetric phase transients associated with the incremental phase shifts.

Before introducing the phase transients we first review the effect of an offset $\Delta\omega$ of the resonance frequency with respect to ω_0. It contributes to the vector-Hamiltonian an additional vector of size $\Delta\omega$ pointing along the z-axis (see Fig. 7). The offset is assumed to be much smaller than both $\Delta\omega_{LG}$ and ω_1. We may, therefore, view the chemical-shift vector $\Delta\omega$ as a perturbation of the main LG vector. To first order, this means that the chemical shift manifests itself as its projection on the LG vector. In the first half of the cycle the projection points in the opposite direction of the LG vector and has a size equal to $\Delta\omega\cos\theta$, where θ is the angle of the LG vector with the $-z$-axis, $\theta = \tan^{-1}(\omega_1/\Delta\omega_{LG})$. Thus the frequency offset effectively adds a vector of size $\Delta\omega\cos\theta$ antiparallel to the LG vector. In the second half of the cycle, the LG vector is inverted while $\Delta\omega$ remains in the positive z direction (see second half in Fig. 7). The effect of the offset is now to add a vector of size $\Delta\omega\cos\theta$ parallel to the LG vector of the second half. The net rotation after a full cycle is consistent with a precession about the LG vector in the $(-x, z)$ quadrant with an effective frequency

$$\omega_{eff} = \Delta\omega\cos\theta. \tag{7}$$

This amounts to a chemical-shift scaling factor of $\cos\theta$. Ideally, θ is the magic angle corresponding to $\cos\theta = 1/\sqrt{3} = 0.577$. However, if the RF deviates from the LG-matched amplitude, the scaling factor is affected. Therefore, RF inhomogeneity across the sample volume causes line broadening that is proportional to the frequency offset. It is a major source of resolution reduction in FSLG and PMLG spectra.

Antisymmetric phase transients contribute an additional component to the effective vector-Hamiltonian. This can be appreciated if we consider the phases of the combined antisymmetric transient pulses at the phase shifts between the pulses. In the first half of the PMLGn sequence the phase shifts are positive and equal to ϕ_{LG}/n. According to Eqs. (1) and (2) the flip angles of the combined transients are thus $\beta_{eff} = 2\beta_a \sin(\phi_{LG}/2n) \sim \beta_a\phi_{LG}/n$ and their phases are the averages of those of the adjacent pulses with the addition of 180°. See the example of PMLG5 shown in Fig. 8, where the full line represents the stepped phase of the pulses and the symbols indicate the phases of the transients. In the second half of the cycle the transients behave similarly, but they are not 180° out of phase with the pulses. There are also two transient pulses at the two points in the cycle where the phase step is 180°. The flip angles of the latter transients are $2\beta_a$, which is much larger than the β_{eff} angles associated with the incremental phase shifts. Their phases are as indicated in Fig. 8.

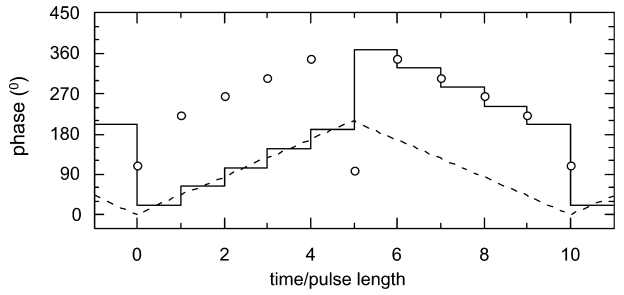

Fig. 8. The full line represents the time dependence of the phase of the RF irradiation during a cycle of PMLG5. The symbols represent the phases of the antisymmetric δ-function transients associated with the phase shifts. The broken line is the angle between the rocking rotating frame and the conventional rotating frame. The phases of the RF irradiation events with respect to the rocking rotating frame are represented by their vertical distances from the broken line.

These phases are all with respect to the conventional rotating frame. To help appreciate their orientations in the rocking rotating frame, the time-dependent phase of the latter with respect to the conventional rotating frame is indicated by a broken line in Fig. 8. We see that the transients, with the exception of those associated with the 180° shifts, represent RF irradiation with a constant phase of 180° in the rocking rotating frame. In both cycle halves it can be approximated as a continuous RF irradiation in the $-x$ direction of the coordinate system of Fig. 7. Its amplitude $\Delta\omega_{\mathrm{tr}}$, expressed in frequency units, is given by the total precession angle of the $n-1$ transients divided by the half-cycle length

$$\Delta\omega_{\mathrm{tr}} \sim ((n-1)/n)\beta_{\mathrm{a}}\phi_{\mathrm{LG}}/\tau_{\mathrm{LG}} \sim \Delta\omega_{\mathrm{LG}}\beta_{\mathrm{a}}. \tag{8}$$

Since this vector $\Delta\omega_{\mathrm{tr}}$ makes an angle $\pi/2-\theta$ with the LG vector, the first-order contribution of the antisymmetric phase transients to the effective frequency is

$$\omega_{\mathrm{eff}} = \Delta\omega_{\mathrm{LG}}\beta_{\mathrm{a}}\sin\theta. \tag{9}$$

As mentioned above, the FSLG limit ($n\to\infty$) is equivalent to RF irradiation that alternates between the two frequencies $\omega_0 \pm \Delta\omega_{\mathrm{LG}}$ with flat phases alternating between 0 and π. In Appendix B it is shown that the same linear RF distortion mechanism that gives rise to pulse transients also creates an extra RF component in the FSLG limit. Moreover, it points along the $-x$ direction of the rocking rotating frame in both cycle halves and its size is given by $\Delta\omega_{\mathrm{LG}}\ \beta_{\mathrm{a}}$, which is exactly equal to the size of $\Delta\omega_{\mathrm{tr}}$ given by Eq. (8) for the case of a small number of relatively large phase steps. This is a justification of the proposition made in the previous section, where we argued that the δ-function approach to the description of pulse transients remains valid for very small pulse lengths.

The antisymmetric transients associated with the 180° shifts are represented by a sudden nutation over angle $2\beta_{\mathrm{a}}$ about the y-axis of the rocking rotating frame at the beginning of the cycle and by a similar nutation about the $-y$-axis at the midpoint of the cycle. This can be verified by inspection of the phases plotted in Fig. 8. Although these nutations are much larger than the individual transient nutations at the small phase shifts, their effect on the net precession is much smaller because of the following. Under conditions where $\omega_{\mathrm{eff}}=0$ and when the RF is matched to the LG condition, the magnetization precesses full circle about the LG vector in the course of half a cycle, so that the two $2\beta_{\mathrm{a}}$ precessions about y and $-y$ exactly cancel each other. When ω_{eff} does not vanish or when the LG condition is not exactly matched, the perturbations of the LG vector are still much smaller than the vector itself. Therefore, the precession over half a cycle does not deviate much from 360°, ensuring continued near cancellation of the two precessions associated with the 180°-shift transients.

We now turn to the amplitude transients. The antisymmetric amplitude transients at the incremental phase steps (see Eqs. (3) and (4)) can similarly be shown to give rise to an apparent magnetic field of size $\Delta\omega_{\mathrm{LG}}\alpha_{\mathrm{a}}$ along the y-axis of the rocking rotating frame, pointing in the same direction in both halves of the cycle. The identical result is obtained for FSLG (Appendix B). Since it is perpendicular to the LG vector, it does not contribute to the effective frequency in first order. Furthermore, the amplitude transients at the two 180° phase jumps in the PMLG cycle generate two precession events about the $\pm x$ directions in the rocking rotating frame. Like the phase transients at these points in time, they compensate each other and do not contribute to the net precession motion.

In summary, the effective frequency of precession under PMLG irradiation is dominated by the frequency offset $\Delta\omega$ and antisymmetric phase transients β_{a} according to

$$\omega_{\mathrm{eff}} = \Delta\omega\cos\theta + \Delta\omega_{\mathrm{LG}}\beta_{\mathrm{a}}\sin\theta, \tag{10}$$

where $\theta = \tan^{-1}(\omega_1/\Delta\omega_{\mathrm{LG}})$. Ideally ω_1 has the value $\Delta\omega_{\mathrm{LG}}\sqrt{2}$ ensuring that θ is the magic angle. A deviation of the RF amplitude from its ideal value,

$$\omega_1 = \Delta\omega_{\mathrm{LG}}\sqrt{2}(1+\varepsilon) \tag{11}$$

induces corrections to $\cos\theta$ and $\sin\theta$. Moreover, since the phase transients are proportional to the RF amplitude (see above), it also changes β_{a} to $\beta_{\mathrm{a}}(1+\varepsilon)$. Working this out to first order in ε gives

$$\omega_{\mathrm{eff}} = (1/\sqrt{3})(1-2\varepsilon/3)\Delta\omega + (1/\sqrt{3})(1+4\varepsilon/3)\omega_1\beta_{\mathrm{a}}. \tag{12}$$

In actual experiments the coefficients of this equation will often deviate from the theoretical values. Therefore, we rewrite Eq. (12) in a more general form as

$$\nu_{\mathrm{eff}} = (\sigma_0+\sigma_1\varepsilon)\Delta\nu + (\eta_0+\eta_1\varepsilon)\nu_1\beta_{\mathrm{a}}, \tag{13}$$

where we switched to a ν-notation of the frequencies to indicate that in experimental situations they are usually

given in Hz. The theoretical values of the main coefficients are $\sigma_0 = 0.577$ (the chemical shift scaling factor), $\eta_0 = 0.0101\,\mathrm{deg}^{-1}$, and their corrections due to RF amplitude deviations are given by $\sigma_1 = -0.38$ and $\eta_1 = 0.013\,\mathrm{deg}^{-1}$. They will be compared with numerical and experimental data in the following sections. The absolute value of ν_{eff} is minimized at the frequency offset where the two terms in Eq. (13) cancel. The position of this minimum depends on β_{a} and, hence, on the probe tuning. A shift of the minimum due to probe detuning was recently reported by Morcombe et al. [25].

Since the two ε terms in Eqs. (12) and (13) are of opposite sign, it is usually possible to set up the spectrometer such that they cancel each other. This has important implications for the inhomogeneity broadening of the spectra. If the RF amplitude is inhomogeneous with a fractional distribution width $\Delta\varepsilon$, Eq. (13) predicts that the PMLG spectrum is broadened by

$$B = |1.33\nu_{\mathrm{eff}}(0) - 0.38\Delta\nu|\Delta\varepsilon, \tag{14}$$

where $\Delta\nu$ is the frequency offset and $\nu_{\mathrm{eff}}(0)$ is the transient-induced effective frequency measured at $\Delta\nu = 0$. The significance of this result is brought out in Fig. 9, where the predicted absolute values of ν_{eff} and B are simultaneously plotted versus $\Delta\nu$. While a phase-transient-generated effective frequency $\nu_{\mathrm{eff}}(0)$ displaces the null point of ν_{eff} to one side of resonance, it causes the inhomogeneity broadening to be nulled at a well-defined offset on the other side of resonance. This explains the generally observed phenomenon that one side of resonance is preferred for best resolution in PMLG and FSLG, and for that matter in many other multiple-pulse experiments (see next section). We have now shown that the offset at which resolution is optimized is a function of the sign and size of the antisymmetric phase transients β_{a}.

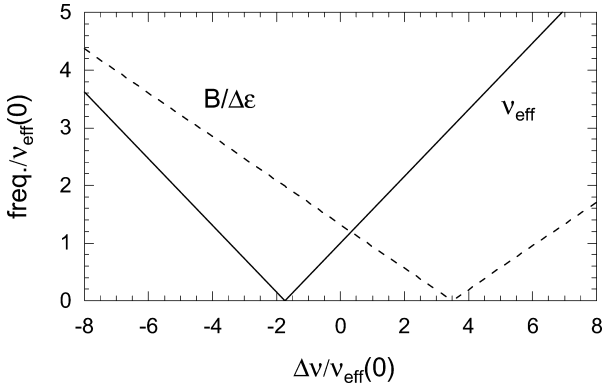

Fig. 9. The effective frequency ν_{eff} and the broadening B of a PMLG signal as function of the frequency offset $\Delta\nu$, as predicted by Eqs. (12)–(14). The broadening is due to a fractional RF-amplitude distribution of width $\Delta\varepsilon$. The plotted quantities are normalized to the on-resonance effective frequency $\nu_{\mathrm{eff}}(0)$, which is due to phase transients.

4. Numerical calculations

The results of the previous section were tested by numerical simulations. A Fortran program was written to calculate the rotation matrix describing the net precession of a magnetization vector over the course of a multiple-pulse cycle by multiplication of the rotations matrices associated with the individual pulses in the proper order. The rotation matrix obtained at the end of the cycle was then analyzed to determine (1) the direction of the effective axis about which the net rotation has occurred and (2) the total angle of precession. Dividing the latter by the cycle time yielded the calculated effective frequency ν_{eff}.

The calculations were performed in the conventional rotating frame. For each pulse the precession is about the combined RF and offset vectors. Each pulse is preceded and followed by its accompanying δ-function transient pulses, which are incorporated in the calculation by performing the specified precessions about the appropriate vectors in the xy plane of the rotating frame. The offset frequency is ignored during δ-function transient pulses. The coinciding trailing and leading transients at the transitions between consecutive pulses are applied one after the other in contrast to the theoretical approach of the previous section, where their combined effect was evaluated separately. The program could also accommodate the BLEW-12 and DUMBO-1 sequences without much modification.

The dependence of the resulting ν_{eff} on $\Delta\nu$, β_{a}, and ε was found to be approximately linear, provided their ranges were kept relatively small ($|\Delta\omega|/\omega_1 < 20\%$, $|\beta_{\mathrm{a}}| < 10°$, and $|\varepsilon| < 5\%$). In this way the equivalents of the coefficients of Eq. (13) could be evaluated. The results are listed in Table 2. The agreement with Eqs. (12) and (13) is quite satisfying. The table also reproduces the published scaling factors for BLEW-12 [6] and DUMBO-1 [14]. It should further be noted that DUMBO-1 has the smallest σ_1 and η_1 coefficients for RF-amplitude dependence, corroborating the finding of its inventors that this pulse cycle is least sensitive to RF inhomogeneity [14]. As to non-linear contributions, the calculations showed that under the simultaneous presence of offset and antisymmetric phase transients the largest deviations from linearity are due to small corrections terms of the form $\Delta\nu\beta_{\mathrm{a}}^2$ and $\Delta\nu^2\beta_{\mathrm{a}}$. There are no contributions from bilinear $\Delta\nu^2$, $\Delta\nu\beta_{\mathrm{a}}$, or β_{a}^2 terms.

Another remarkable result is that for all the sequences listed in Table 2 the broadening mechanisms of RF inhomogeneity associated with offset- and phase-transient shifts (σ_1 and η_1) counteract each other, thus leading to improved resolution on one side of resonance in cases where β_{a} does not vanish, as was illustrated in Fig. 9.

The calculations further provided the orientation of the effective vector-Hamiltonian in the rotating frame.

Table 2
Numerically obtained coefficients describing the effective frequency $\nu_{\text{eff}} = (\sigma_0 + \sigma_1\varepsilon)\Delta\nu + (\eta_0 + \eta_1\varepsilon)\nu_1\beta_a$ due to chemical-shift offset $\Delta\nu$, antisymmetric phase transients β_a, and a fractional deviation ε of the RF amplitude from its ideal value ν_1; and the tilt angle θ of the effective vector-Hamiltonian when $\varepsilon = 0$

Pulse cycle	σ_0	σ_1	η_0[b]	η_1[b]	θ (°)
PMLG*n*, theory[a]	0.577	−0.38	1.01	1.34	55
PMLG3	0.595	−0.43	1.04	1.32	67
PMLG5	0.585	−0.39	1.02	1.35	59
PMLG*n* ($n \geqslant 7$)	0.578 ± 0.02	-0.38 ± 0.02	1.01 ± 0.01	1.34 ± 0.02	56 ± 1
BLEW-12	0.472	−0.33	0.82	1.30	63
DUMBO-1	0.518	−0.21	0.90	0.76	38[c]

[a] From Eq. (12).
[b] η_0 and η_1 are in units of 10^{-2} deg^{-1}.
[c] In agreement with experimental determination [29].

Using the proper phase tables, this vector consistently fell in the x–z plane. Its tilt angle θ with respect to the z-axis was found to be a function of the fractional RF misadjustment ε. Numerical results for θ are listed in Table 2, but only for ideally matched RF. The theoretical model developed for FSLG in the previous section (see discussion of Fig. 7) predicted that the direction of the effective Hamiltonian vector coincides with that of the LG vector irrespective of whether the neat precession is caused by a frequency offset or by phase transients. It is, therefore, not surprising that for PMLG the numerically calculated tilt angles due to offset and phase transients were identical and equal to the magic angle ($\theta \cong 55°$). This allowed us to combine them in one column in Table 2. Remarkably, the respective θ's of offset and phase transients in BLEW and DUMBO are also identical despite the fact that those pulse cycles do not have an obvious equivalent of the LG vector associated with them. Interestingly, Rhim et al. found for the multiple-pulse sequences analyzed by them that the respective vector-Hamiltonians have identical orientations, as well [27,32]. It suggests that there is a fundamental mechanism, not understood by us, which causes the vector-Hamiltonians due to offset and antisymmetric phase transitions to be consistently parallel to each other.

The Fortran program also allows examination of other pulse imperfections. Most were found to affect the vector-Hamiltonian to an insignificant extent. First, we looked at symmetric phase transients, and antisymmetric and symmetric amplitude transients. None of these produced appreciable shifts in the effective frequency. In the case of antisymmetric amplitude transients this is as predicted in the theoretical model. As to symmetric transients, which we described above as problematic entities in the δ-function approximation, it is comforting to find that incorporating them in any of the listed pulse sequences does not make any difference anyway. The numerical results further established that omitting or changing antisymmetric phase transients accompanying the 180° phase shifts does not lead to significant artifacts. This justifies the conclusion made in the theoretical model that the effects of phase transients associated with the 180° phase shifts cancel each other. Similarly, the phase-settling times for the 180° phase shifts in PMLG can be made to differ from the phase-settling times of the incremental phase shifts without penalty.

The only pulse imperfections that produced alterations of the effective frequency were phase errors and the insertion of an observation window like the one employed in *w*PMLG [15]. The combined effect of windows and phase transients on the vector-Hamiltonian is the subject of recent work by Bosman et al. [34]. Phase errors tend to create a Hamiltonian with a component along the y-axis of the rocking rotating frame (compare Fig. 7). It is unlikely that they occur in modern spectrometers. Moreover, a spin-locked signal along the y-axis has not been detected in our experiments.

5. Results

A sample of HMB in a 4 mm MAS rotor with its volume restricted to a 6 mm length was used to verify the theoretical predictions. The RF-amplitude distribution for that sample geometry stretches over an 18% range, as can be seen in the nutation spectrum shown in Fig. 10A (see also Section 7). The PMLG spectra were obtained with the pulse sequence described in Section 7. The detection method was designed such that we measured amplitude modulation along the y-axis of the rotating frame. We first evaluate the effects of pulse transients and RF inhomogeneity. To that end we examine PMLG9 spectra obtained with the carrier frequency kept on resonance ($\Delta\nu = 0$) and with varying probe-tuning frequency ν_{probe}. Use was made of previously determined calibrations curves for β_a versus ν_{probe}, examples of which were shown in Fig. 6. Prior to each spectrum the probe was first tuned to the appropriate frequency and the RF amplitude was adjusted to obtain a PMLG9 frequency scaling factor close to 0.577. Spectra measured for some of the values of β_a are shown in Fig. 10B.

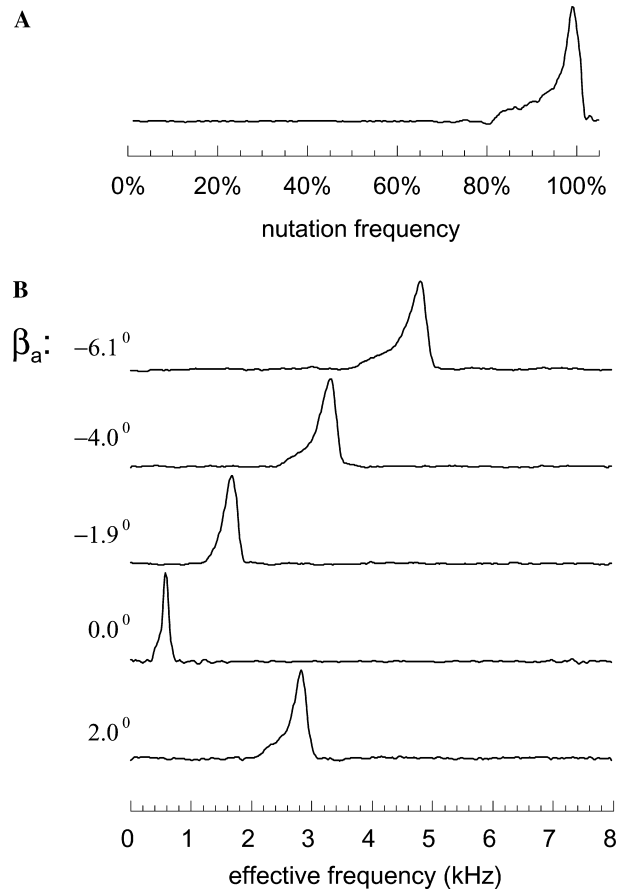

Fig. 10. (A) Nutation spectrum of HMB in a 4 mm MAS rotor with the sample length restricted to 6 mm. (B) PMLG9 lineshapes of the same HMB sample obtained with the carrier frequency on resonance. The probe was tuned at five different frequencies corresponding to the indicated antisymmetric phase transients β_a, which were determined using one of the calibration curves shown in Fig. 6. The elemental pulse length was 0.87 μs, which corresponds to a cycle time $2\tau_{LG} = 15.66$ μs and an LG-matched RF amplitude $\nu_1 = 104$ kHz. The spectra were obtained in 2D mode with t_1 increments of 62.64 μs, equaling four LG cycles. The indirect dimension was processed by real FT without apodization. Spinning speed was 12 kHz. The spectra are affected by t_1 noise possibly related to amplitude fluctuations mentioned in the text.

The main features predicted by the β_a term in Eq. (13) are clearly reproduced. First, the effective frequency of the peak maximum increases with increasing $|\beta_a|$. Second, the lineshapes resemble the nutation spectrum and are wider for larger $|\beta_a|$ values, showing that the broadening is due to the simultaneous presence of transients and RF inhomogeneity. Third, the horizontal polarity of the lineshapes and the nutation spectrum are the same, in agreement with the positive sign of η_1, which predicts that the effective frequency is larger at stronger RF fields. Finally, the absence of zero-frequency signals indicates that there was no spin-locked magnetization component along the y-axis of the rotating frame (see Section 7), verifying that the effective Hamiltonian points in the x–z plane, in accordance with the theory (see Fig. 7).

A quantitative comparison with the η_0 term of Eq. (13) is made in Fig. 11, where the effective frequency of the peak maximum, measured on resonance for HMB, is plotted versus β_a. Included in the plot are two sets of data, which were obtained with different amplifier tuning configurations. They were acquired several weeks apart during which time the probe had been used for other purposes and the amplifier configuration had been changed. The agreement between the two series indicates that the phase-transient behavior, including the adjustment of β_a with the help of a calibration curve, is highly reproducible. In the figure, the data are compared with theoretically predicted curves calculated with the theoretical value $\eta_0 = 0.0101\ \text{deg}^{-1}$. The agreement with the slope is very satisfactory. However, we needed to add a correction term $\beta_0 = 0.65°$ to β_a in order to get the best fit (see formula in figure caption). It is equivalent to the addition of a constant term of 0.68 kHz to the theoretical effective frequency. This corresponds to an error Hamiltonian of that magnitude pointing along the LG vector in Fig. 7. Furthermore, the rounded cusp in Fig. 11 shows that there is another error-Hamiltonian component pointing in a direction perpendicular to the LG vector. Since the spectra obtained around $\beta_a = -0.65$ did not show signs of a spin-locked component (see, for instance, the absence of a zero-frequency signal in the fourth trace in Fig. 10B), we conclude that this error Hamiltonian is also in the xz plane. The perpendicular component loses significance when ν_{eff} is larger than ~2 kHz as a result of second averaging. In Section 6 we return to these small non-predicted contributions to the Hamiltonian.

Next we verified the η_1 term, which describes the combined effects of antisymmetric phase transients and RF inhomogeneity. Eqs. (12) and (13) predict that a plot of the line broadening versus the effective frequency should give a straight line with a slope given by

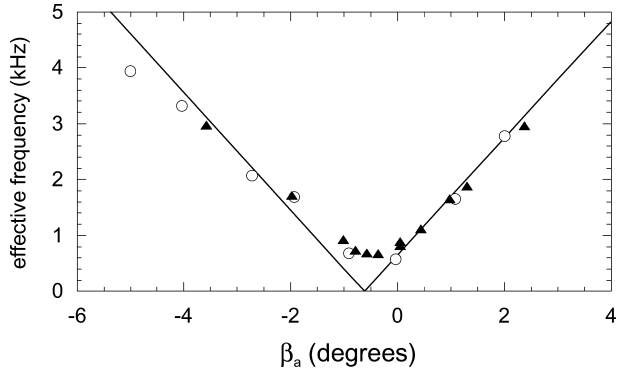

Fig. 11. The effective frequencies of the peak maxima in two sets of on-resonance PMLG9 measurements of HMB as function of the antisymmetric phase transients β_a. The open symbols and closed correspond to the spectra in Fig. 10 and another series, respectively. The straight lines are calculated as $\Delta\nu_{eff} = |\eta_0\nu_1(\beta_a + \beta_0)|$, where $\eta_0 = 0.0101\ \text{deg}^{-1}$, $\nu_1 = 104$ kHz, and $\beta_0 = 0.65°$.

$\Delta\varepsilon\eta_1/\eta_0 = 4\Delta\varepsilon/3$. For $\Delta\varepsilon$ we took the value of 18%, which is the width of the nutation spectrum below the 12% level. To be consistent, the broadenings B of the PMLG9 spectra were measured at 6% of the peak height. At higher intensity levels the contribution of 'natural linewidth' broadening is relatively more pronounced. The resulting plot of B versus ν_{eff}, derived from the spectrum series of Fig. 10, is shown in Fig. 12. A linear curve fit gave a slope of 0.22, in very good agreement with the theoretical value of $(4/3) \times 0.18 = 0.24$. The intersect of 0.20 kHz is the 'natural linewidth' at 6% peak height. It is 1.2 ppm in the chemical-shift-scaled spectrum.

We now turn to the dependence on frequency offset $\Delta\nu$. In order to verify the effects predicted by Fig. 9, the spectra were obtained with a varying offset frequency and a fixed non-zero value of $\beta_a = -1.9°$. The latter was characterized by an on-resonance effective frequency $\nu_{\text{eff}}(0) = 1.28$ kHz and a corresponding width at 6% equal to $B(0) = 0.53$ kHz. PMLG9 spectra obtained at offset intervals of 4 kHz are shown in Fig. 13. The predicted qualitative features are again demonstrated. In particular, we note that most of the lineshapes are now mirror images of the nutation lineshape, in agreement with the negative sign of σ_1. For offsets around $\Delta\nu = 0$, where the transient-related broadening mechanism dominates, the lineshapes are not inverted.

The quantitative results for ν_{eff} and B at 6% height are plotted simultaneously in Fig. 14. The plots clearly reproduce the main features of Fig. 9, in particular the occurrence of ν_{eff} and B minima on opposite sides of resonance. The ν_{eff} curve is similar to results reported by others [25]. The straight lines drawn through the frequency points are curve-fitting result of

$$\nu_{\text{eff}} = |\sigma_0\Delta\nu + \eta_0\nu_1(\beta_a + \beta_0)|. \quad (15)$$

The fitted parameters are $\sigma_0 = 0.575$ (not surprising in view of the fact that the RF amplitude was adjusted to attain that scaling factor), $\eta_0\nu_1 = 1.07$ kHz/deg, $\beta_a = 1.9°$, and $\beta_0 = 0.65°$. This is in perfect agreement with the theoretical predictions, except for the β_0 correction to β_a. It is equal to the β_0 correction needed to get the frequency data to fit in Fig. 11. The broadening data shown in Fig. 14 can similarly be fitted to the corresponding equation,

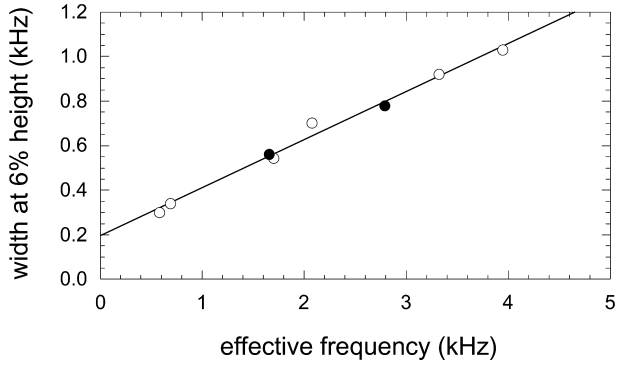

Fig. 12. The width at 6% height of the series of PMLG9 spectra displayed in Fig. 10 plotted against the effective frequency of the peak maximum. The spectra were obtained on resonance ($\Delta\nu = 0$) and with varying β_a. The open and closed symbols are for $\beta_a < 0$ and >0, respectively. The straight line is a fit having a slope of 0.22 and a width–axis intersect of 0.2 kHz.

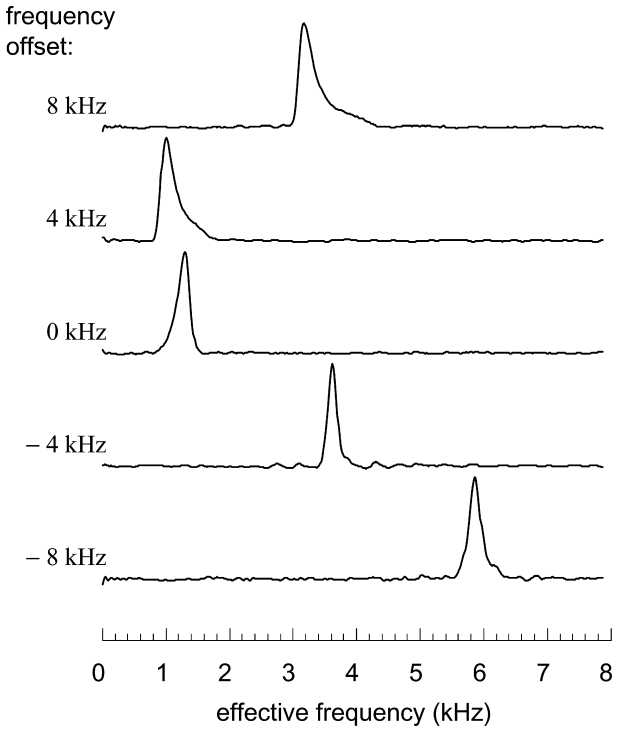

Fig. 13. PMLG9 lineshapes of the same HMB sample as used for Fig. 10. The spectra were taken at different offsets of the resonance frequency of HMB with respect to the carrier frequency as indicated. (Positive $\Delta\nu$ corresponds to a carrier frequency below the carrier frequency.) The probe was tuned at a frequency that gave antisymmetric phase transients with $\beta_a = -1.9°$. Other experimental conditions were as in Fig. 10.

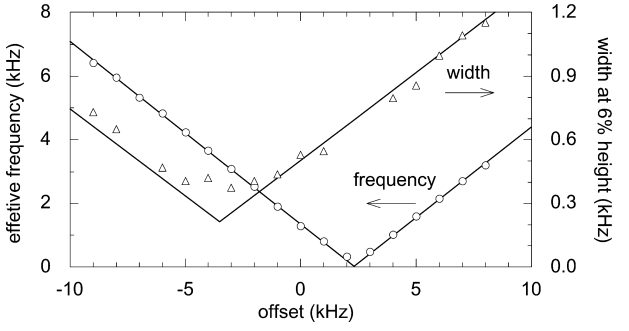

Fig. 14. Frequency-offset dependence of the effective frequency and width at 6% height of the series of PMLG9 spectra displayed in Fig. 13. The spectra were obtained with β_a fixed at −1.9°. The spectra around the frequency minimum at 2.4 kHz offset were artificially narrowed by folding of the lineshape onto itself. Their widths are omitted from the plot. The straight lines are curve fits described in the text.

$$B = \Delta\varepsilon|\sigma_1\Delta\nu + \eta_1\nu_1(\beta_a + \beta_0)| + B_{nat}, \quad (16)$$

where $\Delta\varepsilon$ is set equal to 18% and where the term B_{nat} is introduced to represent the 'natural linewidth.' The fitted parameters are $\sigma_1 = -0.46$, $\eta_1\nu_1 = 1.3$ kHz/deg, $\beta_0 = 0.65°$, and $B_{nat} = 0.21$ kHz. The σ_1 coefficient deviates from the theoretical value of −0.38. This is due to the large size of $\Delta\varepsilon$, which falls outside the range where the ν_{eff} dependence on ε is linear. A numerical calculation for $\Delta\varepsilon = 18\%$ gave $\sigma_1 = -0.46$, in perfect agreement with experiment. The coefficient $\eta_1\nu_1$ describing the β_a dependence of the broadening also deviates from the theoretical value 1.38 kHz/deg, but not severely. The 'natural linewidth' is close to the 0.20 kHz found above when we studied the width as function of β_a. The rounding of the cusp at the minimum of the width curve represents in addition to the 'natural linewidth' a broadening of about 0.16 kHz at 6% height.

6. Discussion

Disregarding a few residual artifacts, the experimental results agree quite well with the quantitative theoretical and numerical predictions. We view this as a justification of the two assumptions underlying the theory, i.e., (1) the transients are due to linear pulse distortions and (2) they can be described as antisymmetric δ-function pulses at the beginning and end of each irradiation period of constant amplitude and phase. The results were admittedly acquired on a 300 MHz instrument but we fully expect higher-field spectrometers to behave similarly. Nevertheless, the results did not agree completely with the predictions. The following discussion addresses the origins of the deviations.

The assumption of the linear character of the transients relates to the RF currents in the sample coil. No observations were made that contradict its validity. On the other hand, the δ-function assumption, which relates to the way the nuclear spins respond to the transients, leads to identifiable deficiencies. One is the ambiguity of the concept of symmetric pulse transients discussed above in Section 2. Another is the need to add a correction term $\beta_0 = 0.65°$ to the antisymmetric phase transient β_a in order to obtain agreement with the theoretical predictions for PMLG9. Both discrepancies are higher-order corrections related to the non-commutativity of precessions, which causes the effects of phase transients to be dependent on the prevailing bulk RF irradiation with which they coincide. It is the reason why the flip angle β_a that quantitates the antisymmetric phase transient experienced in association with isolated 180° pulses differs slightly from the corresponding flip angle $\beta_a + \beta_0$ quantitating its effect in association with the phase increments of PMLG. Fortunately, the deviations caused by the ambiguities of the δ-function approximation are relatively small and can, at least in the case of PMLG9, easily be taken into account by the β_0 correction. We have not yet evaluated its size for the other phase-modulated sequences.

Other deviations from theoretical predictions are less well understood. In particular, we do not know the origin of the extra line broadening at offsets where the inhomogeneity broadening is smallest (rounding of the cusp at the minimum of the width curve in Fig. 14). It is larger than the residual broadening found when $\Delta\nu = 0$ and $\beta_a = -\beta_0$ (Figs. 10 and 12). We did not yet investigate if it is due to RF inhomogeneity or another broadening mechanism. One possibility could be the fluctuating RF amplitude of our spectrometer (see Section 7) but this was neither properly investigated. The other poorly understood phenomenon is the vector-Hamiltonian perpendicular to the LG vector, which gives rise to a small effective frequency when $\Delta\nu = 0$ and $\beta_a = -\beta_0$ (Figs. 10 and 11). Fortunately, the impact of this error Hamiltonian is canceled by second averaging if the effective frequency is large enough. Its existence is one reason to perform PMLG with the carrier frequency outside the chemical shift region of interest [25]. An additional advantage of working off-resonance is being able to produce cosine modulation in the indirect 2D dimension without implementation of TPPI or hypercomplex data processing (see Section 7).

The major conclusion of the present work is that the antisymmetric portion of the phase transients and the RF inhomogeneity are the only pulse imperfections having appreciable impact on CRAMPS spectroscopy in modern spectrometers. Since the antisymmetric transient has a size β_a that is a function of the frequency at which the probe gives minimum reflection, its effects on the spectra are fully controllable within an allowable tuning range. A result of practical importance is that for each value of β_a a matching frequency offset $\Delta\nu$ exists for which the line broadening due to RF inhomogeneity is greatly reduced. This suggests that under such conditions severe restriction of the sample volume may not be a necessity.

A practical approach to setting up for optimal conditions is suggested in the following example. Although it is presented specifically for PMLG, it is equally applicable to FSLG (according to the conclusions of Appendix B) and to BLEW-12 and DUMBO-1 (according to numerical results.) Recognizing that the transients depend on the probe performance, which in turn is often influenced by insertion of the sample, the use of a calibration curve for β_a is in general not the most efficient method. (We relied on it in this paper only for the purpose of a comprehensive investigation and we were able to do so because we did not use more than one sample.) A more direct method is to begin with taking two PMLG spectra, one with the carrier frequency on

resonance and one shifted by, say, 20 ppm. The difference in effective frequencies gives the scaling factor σ_0, which can be adjusted to 0.577 by changing the RF amplitude accordingly (multiply the RF amplitude by $\sqrt{2\sigma_0^2/(1-\sigma_0^2)}$). The effective frequency obtained on resonance, $\nu_{\text{eff}}(0)$, reveals the value of $(\beta_a + \beta_0)$. Solving Eq. (16) for $B = B_{\text{nat}}$ gives the offset for optimum narrowing of the RF inhomogeneity broadening: $\Delta\nu = \nu_{\text{eff}}(0)\eta_1/(\sigma_1\eta_0) = 2.6\nu_{\text{eff}}(0)$, where we substituted the experimentally determined coefficients. The sign of $\Delta\nu$ is easily found by the condition that the ν_{eff} minimum should be on the other side of resonance. If $\Delta\nu$ turns out to be larger than experimentally convenient, one can retune the probe at another frequency and repeat this routine until a desired spectrometer setup is found. We followed this protocol with glycine confined to a 6 mm sample length in a 4 mm rotor spinning at 12 kHz, using a double-resonance ^{1}H/^{19}F probe operating at 300 and 282 MHz. A β_a calibration curve had not been measured. In fact, the transients in this probe are not reproducible because of the closeness of the two frequencies and the strong influence of the internal filters. With the probe tuned close to resonance (300.12 MHz) we measured $\nu_{\text{eff}}(0) = 1.73$ kHz. It required $\Delta\nu = 4.5$ kHz for optimum resolution, which we found somewhat large. Changing the probe tuning to 300.3 MHz reduced $\nu_{\text{eff}}(0)$ to 1.09 kHz, which allowed spectra to be taken at 2.8 kHz off resonance. Other than a final adjustment of the RF amplitude, no other adjustments were made. The resulting PMLG9 spectrum of glycine at 12 kHz MAS speed is shown in Fig. 15.

So far we have considered the linewidth at 6% height. A more common measure of spectral resolution is the full width at half height (FWHH). In the nutation spectrum it is about 3.5%, which is one-fifth of the total width at 6% height. In the HMB spectra plotted in Figs. 10 and 13 the FWHH ranges from 0.12 to 0.36 kHz. While it follows the same trend as the width at 6% height, its dependence on $\Delta\nu$ and β_a is less pronounced because of the larger relative contribution of the 'natural' FWHH. It implies that for frequency offsets in the region where the width is at a minimum, the inhomogeneity contribution to the FWHH is negligible. This appears to be the case for the offset-optimized glycine spectrum of Fig. 15. Curve fitting to Lorentzian lineshapes gives FWHH between 0.10 and 0.14 kHz, corresponding to 0.6 and 0.8 ppm (scaled) at 300 MHz.

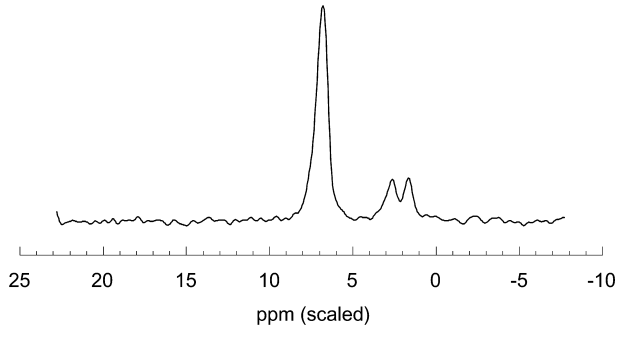

Fig. 15. PMLG9 spectrum of glycine obtained after the setup procedure described in the text. RF amplitude inhomogeneity was 18% across the sample volume. Spinning speed was 12 kHz. PMLG9 full cycle time was 15.66 μs. The spectra were obtained in 2D mode with 128 t_1 increments of 93.96 μs, equaling four LG cycles. No apodization was applied in the indirect dimension. The spectrum is shown in skyline projection. It is affected by t_1 noise possibly related to amplitude fluctuations mentioned in the text.

7. Experimental

The experiments were performed with a Chemagnetics Infinity spectrometer operating at 300 MHz for protons. Its transmitter power amplifier is the Chemagnetics CMA module having tunable and matchable input and output resonant circuits with a Q-factor of about 100. For the NMR measurements we used the proton channel of a Varian/Chemagnetics HXY triple resonance probe with 4 mm ceramic magic-angle-spinning rotors. The tuning curve of the probe as measured with a Wavetek frequency sweeper and a directional coupler is about 1 MHz wide at the 3 db level, consistent with a Q-factor of about 300 [41]. The sample used was hexamethylbenzene (HMB). It was chosen because of its relatively small dipolar broadening, its short T_1 relaxation time of 0.3 s, and the simplicity of its single-resonance proton spectrum.

The wire windings of the sample coil are equally spaced over a length of 12 mm. The sample volume in the rotor was confined to a length of 6 mm around the center of the coil. A measurement of pulse flip angles of a small liquid sample placed at various axial positions revealed that the RF amplitude ω_1 as a function of the position has a broad maximum $\omega_{1\,\max}$ at the center of the coil and drops to about 82% at a distance of ±3 cm. Over the full conventional sample volume of 12 mm length, the RF amplitude drops to 40% at the edges. The ω_1 dependence on the axial position can roughly be described by a parabola. It corresponds to an inhomogeneity distribution $P(\omega_1) \propto \sqrt{\omega_{1\,\max} - \omega_1}$ between $0.82\omega_{1\,\max}$ and $\omega_{1\,\max}$, which has the same profile as the NMR lineshape of an axially symmetric chemical-shift tensor. Its average is 95% of $\omega_{1\,\max}$. The theoretical nutation spectrum for this RF distribution is proportional to $\omega_1 P(\omega_1)$, where the factor ω_1 is intended to account for the varying detection efficiency across the sample volume. A nutation spectrum resembling this shape was indeed obtained experimentally (Fig. 10A). The RF amplitude fluctuates by at least 1% over periods of the order of minutes. Instability of the RF amplifier is a possible source [43]. It is possible that this instability

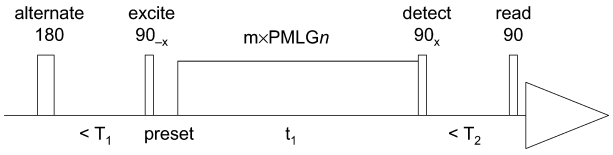

Fig. 16. The pulse sequence used in this work. The 180° pulse is applied before every second acquisition in concert with an alternating detection phase to suppress probe background signals. Combined with CYCLOPS cycling of the read pulse (see text) the phase cycle has eight steps. The PMLG phases are set prior to the pulses by a preset time of 0.2 μs.

contributes the t_1 noise in the spectra shown in the figures, particularly in the nutation spectrum (Fig. 10A).

The PMLG*n* experiments (Fig. 16) were executed in 2D mode. The $90°_{-x}$ excitation pulse prepares the magnetization along y, which is perpendicular to the effective vector-Hamiltonian in all encountered cases. A zero-frequency signal due to spin locking is thereby avoided. The $90°_{x}$ detection pulse places the y-component of the magnetization emerging from PMLG along z. The phases of the read pulse and the detection are CYCLOPS cycled to ensure that the y-component emerging from PMLG is selectively detected. This method yields cosine modulation of the signal as a function of the evolution time, so that real FT of the indirect dimension gives pure absorption spectra. To avoid folding, the carrier frequency must be outside the spectral range.

8. Conclusion

We proposed an explanation for the often-observed asymmetric spectral resolution on opposite sides of resonance in CRAMPS experiments for homonuclear decoupling. The difference in the line broadening is found to be caused by RF amplitude inhomogeneity in the presence of antisymmetric phase transients of the RF irradiation. Phase transients and chemical-shift offsets are similar in that they cause peak shifts in multiple-pulse spectra. Both also lead to RF-inhomogeneity broadening that is proportional to the shift they generate. However, they differ in that the broadening mechanisms associated with offset and phase-transients counteract each other when the offset and the transients are increased. This has the effect that for non-vanishing transients a well-defined offset frequency exists at which the inhomogeneity broadening is greatly reduced. Since the phase transients depend on the probe tuning, the offset at which broadening is minimized can be manipulated by the spectroscopist. A protocol for setting up the spectrometer to achieve optimum conditions is proposed. These results suggest that severe sample volume restriction is not a necessity for improved resolution.

The theory of the effects of offset, pulse transients, and RF inhomogeneity on phase-modulated multiple-pulse spectra is worked out in detail for PMLG. Experimental verification is provided for PMLG9. Theoretical and numeric evidence further indicate that the pulse sequences FSLG, DUMBO-1, and BLEW-12 behave similarly. The theoretical arguments are based on two basic assumptions concerning pulse transients. One is that they are caused by linear RF distortions generated by electronic components of the RF circuits. The other is that transients approximated as δ-function pulses are additive when they coincide at phase shifts during continuous irradiation. In this approximation symmetric transients cannot exist. Deviations from this model occur but measurements showed that they are small. Moreover, the deviations depend on the details of the pulse sequence. For instance, apparent symmetric phase transients are detected mainly in association with isolated pulses. Likewise, fine tuning the spectrometer for vanishing transients with the use of a sequence of isolated pulses does not guarantee their absence in phase-modulated multiple-pulse schemes.

Acknowledgments

This work was inspired by the author's experience in the laboratory of the late Robert W. Vaughan at Caltech in the mid-1970s. Skillful experimental assistance of Robert O. Balback is gratefully acknowledged. The author had stimulating discussions with Professors Kurt W. Zilm and Shimon Vega and Dr. Charles E. Bronniman. He thanks Professors Zilm and Vega for access to preprints of papers by their research groups.

Appendix A. Lack of synchronization between RF and pulse shaping as a source of symmetric pulse transients

The thought experiment of two consecutive identical RF pulses described in the first paragraph of Section 2 tacitly assumed that the timings of the leading and falling edges of the ideal pulse envelopes were such that they occurred at the same phase *within* an RF cycle. If this is not so, there must be a minimum gap between two pulses that are identical in all respects other than in the time at which they begin, as is illustrated in Fig. 17. Eliminating the gap would force the pulses to have different phases.

Mehring and Waugh [40] pointed out that transients of a rectangular pulse distorted by an RLC circuit contain components that depend on the phases *within* the RF cycles at which a pulse begins and ends. These components are in general not the inverse of each other and thus create symmetric transients. Similarly, it is evident from Fig. 17 that in a case where the beginning

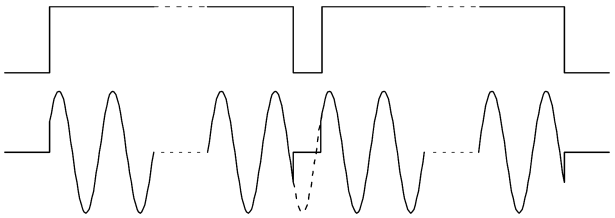

Fig. 17. The leading and trailing sections of two consecutive identical rectangular RF pulses. (Top) The pulse envelopes. (Bottom) The RF oscillation. The drawing demonstrates that when the pulses have the same RF phase while their leading and trailing edges occur at different phases within the RF cycle, there must be a minimum time delay separating the pulses.

and ending phases differ, the trailing transient of the first pulse and the inverted leading transient of the second pulse are not exactly identical. They differ by the response originating from the omitted input RF signal in the gap. It is, however, such a small effect that it can safely be neglected, as has been demonstrated by Barbara et al. [38]. Indeed, Mehring and Waugh's [40] calculations showed that its contribution to the transients is about $4Q$ times smaller than the main antisymmetric portion of the transients, Q being the Q-factor of the RLC circuit.

Appendix B. Linear response theory applied to a continuous phase ramp

The response signal $R(t)$ of a linear system is related to the input signal $I(t)$ by the integral equation

$$R(t) = \int_0^\infty \rho(t')I(t-t')\,\mathrm{d}t', \tag{B.1}$$

where $\rho(t)$ is the response function of the system. In the case of the leading edge of a rectangular RF pulse we have $I(t) = 0$ for $t < 0$ and $I(t) = \mathrm{e}^{\mathrm{i}\omega_0 t}$ for $t > 0$. The response is the RF irradiation experienced by the spins in the sample coil. It can be written as

$$R(t) = \omega_1[1-\theta(t)]\,\mathrm{e}^{\mathrm{i}\omega_0 t}, \tag{B.2}$$

where $\theta(t)$ is the leading-edge transient function consisting of a real in-phase and an imaginary 90°-out-of-phase component, like in the example of Fig. 1A. For simplicity we omit an amplitude coefficient for $I(t)$ and a steady-state phase shift between $I(t)$ and $R(t)$. The transient function $\theta(t)$ starts at $\theta(0) = 1$ and decays to 0 with a decay time τ_{tr}. The integral of $\theta(t)$ corresponds to the first-order δ-function transient pulses defined in this paper,

$$\omega_1 \int_0^\infty \theta(t)\,\mathrm{d}t = \alpha_\mathrm{a} - \mathrm{i}\beta_\mathrm{a}. \tag{B.3}$$

Equating Eqs. (B.1) and (B.2) leads to the relation between $\theta(t)$ and $\rho(t)$,

$$\omega_1[1-\theta(t)] = \int_0^t \rho(t')\,\mathrm{e}^{-\mathrm{i}\omega_0 t'}\,\mathrm{d}t' \tag{B.4}$$

and its derivative

$$\rho(t) = -\omega_1\,\mathrm{e}^{\mathrm{i}\omega_0 t}(\mathrm{d}\theta/\mathrm{d}t). \tag{B.5}$$

Let us now consider an input pulse at a frequency that differs by an offset $\Delta\omega$ from the frequency for which the response function is defined, i.e.,

$$I(t) = \mathrm{e}^{\mathrm{i}(\omega_0+\Delta\omega)t}. \tag{B.6}$$

After a transient period of duration τ_{tr} at the onset of the pulse the following steady state is reached,

$$R(t) = \int_0^\infty \rho(t')\,\mathrm{e}^{\mathrm{i}(\omega_0+\Delta\omega)(t-t')}\,\mathrm{d}t'. \tag{B.7}$$

Substitution of Eq. (B.5) gives

$$R(t) = -\omega_1\,\mathrm{e}^{\mathrm{i}(\omega_0+\Delta\omega)t}\int_0^\infty (\mathrm{d}\theta/\mathrm{d}t')\,\mathrm{e}^{-\mathrm{i}\Delta\omega t'}\,\mathrm{d}t', \tag{B.8}$$

which by partial integration leads to

$$R(t) = \omega_1\,\mathrm{e}^{\mathrm{i}(\omega_0+\Delta\omega)t}\left\{1 - \mathrm{i}\Delta\omega\int_0^\infty \theta(t')\,\mathrm{e}^{-\mathrm{i}\Delta\omega t'}\,\mathrm{d}t'\right\}. \tag{B.9}$$

In practical situations $\Delta\omega\tau_{\mathrm{tr}}$ is smaller than 2π (e.g., $\Delta\omega/2\pi = 100\,\mathrm{kHz}$ and $\tau_{\mathrm{tr}} = 0.3\,\mu\mathrm{s}$ give $\Delta\omega\tau_{\mathrm{tr}}/2\pi = 0.03$). Therefore, $\mathrm{e}^{-\mathrm{i}\Delta\omega t'}$ under the integral of Eq. (B.9) may in first approximation be replaced by 1, giving a simple integration of $\theta(t')$ in Eq. (B.9). According to Eq. (B.3) it can be replaced by the δ-function flip angles, ultimately yielding

$$R(t) = \mathrm{e}^{\mathrm{i}(\omega_0+\Delta\omega)t}\{\omega_1 - \Delta\omega(\mathrm{i}\alpha_\mathrm{a} + \beta_\mathrm{a})\}. \tag{B.10}$$

This shows that the conversion factor ω_1 describing the steady-state response to input radiation at frequency ω_0 is modified to the expression in curly brackets when the input frequency is shifted to $\omega_0 + \Delta\omega$. It further shows how the modified conversion factor is related to the transients of a rectangular pulse at ω_0: The antisymmetric out-of-phase transients produce an RF component that is in phase with the unmodified RF, while the in-phase amplitude gradients produce an out-of-phase component.

Applying this to the first half of an FSLG cycle in continuous phase-ramp mode we note that the RF input is equivalent to irradiation at an offset frequency $\Delta\omega_{\mathrm{LG}}$, which causes the RF amplitude to be reduced by an amount equal to

$$\Delta\omega_{\mathrm{tr}} = \Delta\omega_{\mathrm{LG}}\beta_\mathrm{a}. \tag{B.11}$$

This is exactly the same result as found for small numbers of finite phase increments, as can be seen in Eq. (8) and as is illustrated in Figs. 7 and 8. Similarly, the amplitude transients give rise to an out-of-phase RF component equal to that found for finite phase increments. In the second half of the cycle, where $\Delta\omega_{\mathrm{LG}}$ has a

negative sign, the amplitude is enhanced by the same amount as given in Eq. (B.11).

The approximation made in this derivation is equivalent to the first-order δ-function approximation made in the body of this paper. An appreciation of the neglected contribution is obtained by replacing $e^{-i\Delta\omega t'}$ under the integral of Eq. (B.9) by $1 - i\Delta\omega t'$ instead of by 1. It adds a real and an imaginary term to the expression in the curly brackets of Eq. (B.10). The correction term that is in phase with the unmodified RF (the real term) originates in the in-phase part of $\theta(t)$. Thus in higher-order corrections, the amplitude transients contribute to β_a. A similar derivation can be made for higher-order contributions to the apparent β_a associated with isolated 180° pulses or with the phase increments in PMLG. The corrections depend on the details of the prevailing undistorted irradiation. It is the cause of discrepancies between quantitative evaluations of antisymmetric phase transients under different experimental conditions. A primary example in this paper is the β_0 correction to β_a that was introduced in Eqs. (15) and (16) to fit PMLG results to the theory.

References

[1] M. Lee, W.I. Goldburg, Nuclear magnetic resonance line narrowing by rotating rf fields, Phys. Rev. A 140 (1965) 1261–1271.

[2] J.S. Waugh, L.M. Huber, U. Haeberlen, Approach to high resolution NMR in solids, Phys. Rev. Lett. 20 (1968) 180–183.

[3] P. Mansfield, M.J. Orchard, D.C. Stalker, K.H.B. Richards, Symmetrized multipulse nuclear magnetic resonance experiments in solids. Measurement of the chemical-shift shielding tensor in some compounds, Phys. Rev. B 7 (1973) 90–105.

[4] W.-K. Rhim, D.D. Elleman, R.W. Vaughan, Enhanced resolution for solid state NMR, J. Chem. Phys. 58 (1973) 1772–1773; Analysis of multiple pulse NMR in solids, J. Chem. Phys. 59 (1973) 3740–3749.

[5] D.P. Burum, W.K. Rhim, Analysis of multiple pulse NMR in solids III, J. Chem. Phys. 71 (1979) 944–956.

[6] D.P. Burum, M. Linder, R.R. Ernst, Lower-power multiple line narrowing in solid-state NMR, J. Magn. Reson. 44 (1981) 173–188.

[7] A. Bielecki, A.C. Kolbert, M.H. Levitt, Frequency-switched pulse sequences: homonuclear decoupling and dilute spin NMR in solids, Chem. Phys. Lett. 155 (1989) 341–346.

[8] A. Bielecki, A.C. Kolbert, H.S.M. de Groot, R.G. Griffin, M.H. Levitt, Frequency-switched Lee–Goldburg sequences in solids, Adv. Magn. Reson. 14 (1990) 111–124.

[9] K. Takegoshi, C.A. McDowell, A "magic echo" pulse sequence for the high-resolution NMR spectra of abundant spins in solids, Chem. Phys. Lett. 116 (1985) 100–104.

[10] M. Hohwy, P.V. Bower, H.J. Jakobsen, N.C. Nielsen, A high-order and broadband CRAMPS experiment using z-rotational decoupling, Chem. Phys. Lett. 273 (1997) 297–303.

[11] E. Vinogradov, P.K. Madhu, S. Vega, High-resolution proton solid-state NMR spectroscopy by phase-modulated Lee–Goldburg experiment, Chem. Phys. Lett. 314 (1999) 443–450.

[12] E. Vinogradov, P.K. Madhu, S. Vega, A bimodal Floquet analysis of phase modulated Lee–Goldburg high resolution proton magic angle spinning NMR experiments, Chem. Phys. Lett. 329 (2000) 207–214.

[13] E. Vinogradov, P.K. Madhu, S. Vega, Phase modulated Lee–Goldburg magic angle spinning proton nuclear magnetic resonance experiments in the solid state: a bimodal Floquet theoretical treatment, J. Chem. Phys. 115 (2001) 8983–9000.

[14] D. Sakellariou, A. Lesage, P. Hodgkinson, L. Emsley, Homonuclear dipolar decoupling in solid-state NMR using continuous phase modulation, Chem. Phys. Lett. 319 (2000) 253–260.

[15] E. Vinogradov, P.K. Madhu, S. Vega, Proton spectroscopy in solid state NMR with windowed phase modulated Lee–Goldburg decoupling sequences, Chem. Phys. Lett. 354 (2002) 193–202.

[16] B.C. Gerstein, R.G. Pembleton, R.C. Wilson, L.M. Ryan, High resolution NMR in randomly oriented solids with homonuclear dipolar broadening: combined multiple pulse NMR and magic angle spinning, J. Chem. Phys. 66 (1977) 361–362.

[17] B.-J. van Rossum, H. Förster, H.J.M. de Groot, High field and high-speed CP-MAS ^{13}C NMR heteronuclear dipolar-correlation spectroscopy of solids with frequency-switched Lee–Goldburg homonuclear decoupling, J. Magn. Reson. 124 (1997) 516–519.

[18] A. Lesage, D. Sakellariou, S. Steuernagel, L. Emsley, Carbon-proton chemical shift correlation in solid-state NMR by through-bond multiple quantum spectroscopy, J. Am. Chem. Soc. 120 (1998) 13194–13201.

[19] X.L. Yao, K. Schmidt-Rohr, M. Hong, Medium- and long-distance ^{1}H–^{13}C heteronuclear correlation NMR in solids, J. Magn. Reson. 149 (2001) 139–143.

[20] V. Ladizhansky, M. Veshtort, R.G. Griffin, G. Robert, NMR determination of the torsion angle ψ in α-helical peptides and proteins: the HCCN dipolar correlation experiment, J. Magn. Reson. 154 (2002) 317–324.

[21] B. Alonso, I. Klur, D. Massiot, Studies of surfaces through probe adsorption and solid-state NMR, Chem. Commun. 8 (2002) 804–805.

[22] M. Hong, X. Yao, K. Jakes, D. Huster, Investigation of molecular motions by Lee–Goldburg cross-polarization NMR spectroscopy, J. Phys. Chem. B 106 (2002) 7355–7364.

[23] K. Yamauchi, S. Kuroki, I. Ando, The amide proton NMR chemical shift and hydrogen-bonded structure of glycine-containing peptides and polypeptides in the solid state as studied by multi-pulse-associated high-speed MAS ^{1}H NMR, J. Mol. Struct. 602–603 (2002) 6–16.

[24] V. Chevelkov, B.-J. Van Rossum, F. Castellani, K. Rehbein, A. Diehl, M. Howhy, S. Steuernagel, F. Engelke, H. Oschkinat, B. Reif, ^{1}H detection in MAS solid-state NMR spectroscopy of biomacromolecules employing pulsed field gradients for residual solvent suppression, J. Am. Chem. Soc. 125 (2003) 7788–7789.

[25] C.R. Morcombe, E.K. Paulson, V. Gaponenko, R.A. Byrd, K.W. Zilm, ^{1}H–^{15}N correlation spectroscopy of nanocrystalline proteins, private communication.

[26] U. Haeberlen, High resolution NMR in solids: selective averaging, Adv. Magn. Reson. 1 (1976) 1–190.

[27] M. Mehring, High Resolution NMR Spectroscopy in Solids, Springer-Verlag, Berlin, 1976.

[28] P. Charmont, A. Lesage, S. Steuernagel, F. Engelke, L. Emsley, Sample restriction using magnetic field gradients in high-resolution solid-state NMR, J. Magn. Reson. 145 (2000) 334–339.

[29] A. Lesage, D. Sakellariou, S. Hediger, B. Elena, P. Charmont, S. Steuernagel, L. Emsley, Experimental aspects of proton NMR spectroscopy in solids using phase-modulated homonuclear dipolar decoupling, J. Magn. Reson. 163 (2003) 105–113.

[30] D.E. Demco, S. Hafner, H.W. Spiess, J. Magn. Reson. A 116 (1995) 36.

[31] P.K. Madhu, X. Zhao, M.H. Levitt, Chem. Phys. Lett. 346 (2001) 142–148.
[32] W.-K. Rhim, D.D. Elleman, L.B. Schreiber, R.W. Vaughan, Analysis of multiple pulse NMR in solids. II, J. Chem. Phys. 60 (1974) 4595–4604.
[33] E. Vinogradov, P.K. Madhu, S. Vega, Strategies for high-resolution proton spectroscopy in the NMR of solid-state, Topics in Current Chemistry, Springer, Heidelberg, Germany, in press.
[34] L. Bosman, P.K. Madhu, S. Vega, E. Vinogradov, Radio frequency imperfections in windowed phase modulated Lee–Goldburg decoupling experiments, J. Magn. Reson. 169 (2001) 39–48.
[35] S. Vega, Floquet theory, in: D.M. Grant, R.K. Harris (Eds.), The Encyclopedia of Nuclear Magnetic Resonance, Wiley, London, 1997, pp. 2011–2025.
[36] J.D. Ellett Jr., M.G. Gibby, U. Haeberlen, L.M. Huber, M. Mehring, A. Pines, J.W. Waugh, Spectrometers for multiple-pulse NMR, Adv. Magn. Reson. 5 (1971) 117–176.
[37] R.S. Vaughan, D.D. Elleman, L.M. Stacey, W.-K. Rhim, J.W. Lee, A simple, low power, multiple pulse NMR spectrometer, Rev. Sci. Instrum. 43 (1972) 1356–1364.
[38] T.M. Barbara, J.F. Martin, J.G. Wurl, J. Magn. Reson. 93 (1991) 497.
[39] M. Caravetta, M. Eden, O.G. Johanessen, H. Luthman, P.J.E. Verdegem, J. Lugtenburg, A. Sebald, M.H. Levitt, Estimation of carbon–carbon bond lengths and medium-range internuclear distances by solid-state nuclear magnetic resonance, J. Am. Chem. Soc. 123 (2001) 10628–10638.
[40] M. Mehring, J.S. Waugh, Phase transients in pulsed NMR spectrometers, Rev. Sci. Instrum. 43 (1972) 649–653, The relevant coefficients $1/(4Q)$ in Eqs. (13) and (15) were unfortunately typeset as $(1/4)Q$.
[41] E.M. Purcell, Electricity and Magnetism, McGraw-Hill, New York, 1963 (Chapter 8).
[42] S.L. Patt, Single- and multiple-frequency-shifted laminar pulses, J. Magn. Reson. 96 (1992) 94–102.
[43] C.E. Bronniman, Varian Inc., private communication.